

# Radiatively Active Hydrometeors Frequencies from CloudSat-CALIPSO Data for Evaluating Cloud Fraction in Global Climate Models

Jui-Lin F. Li<sup>1</sup>, Wei-Liang Lee<sup>2</sup>, Kuan-man Xu<sup>3</sup>, Yu Cian Tsai<sup>4</sup>, Jonathan H Jiang<sup>5</sup>, Jia-Yuh Yu<sup>6</sup>, Graeme Stephens<sup>7</sup>, Eric J. Fetzer<sup>8</sup>, and Wei-Ting Chen<sup>9</sup>

<sup>1</sup>JPL/CalTech/NASA

<sup>2</sup>Academia Sinica

<sup>3</sup>NASA Langley

<sup>4</sup>Department of Atmospheric Sciences, National Central University

<sup>5</sup>Jet Propulsion Laboratory, California Institute of Technology

<sup>6</sup>National Central University

<sup>7</sup>JPL/Caltech

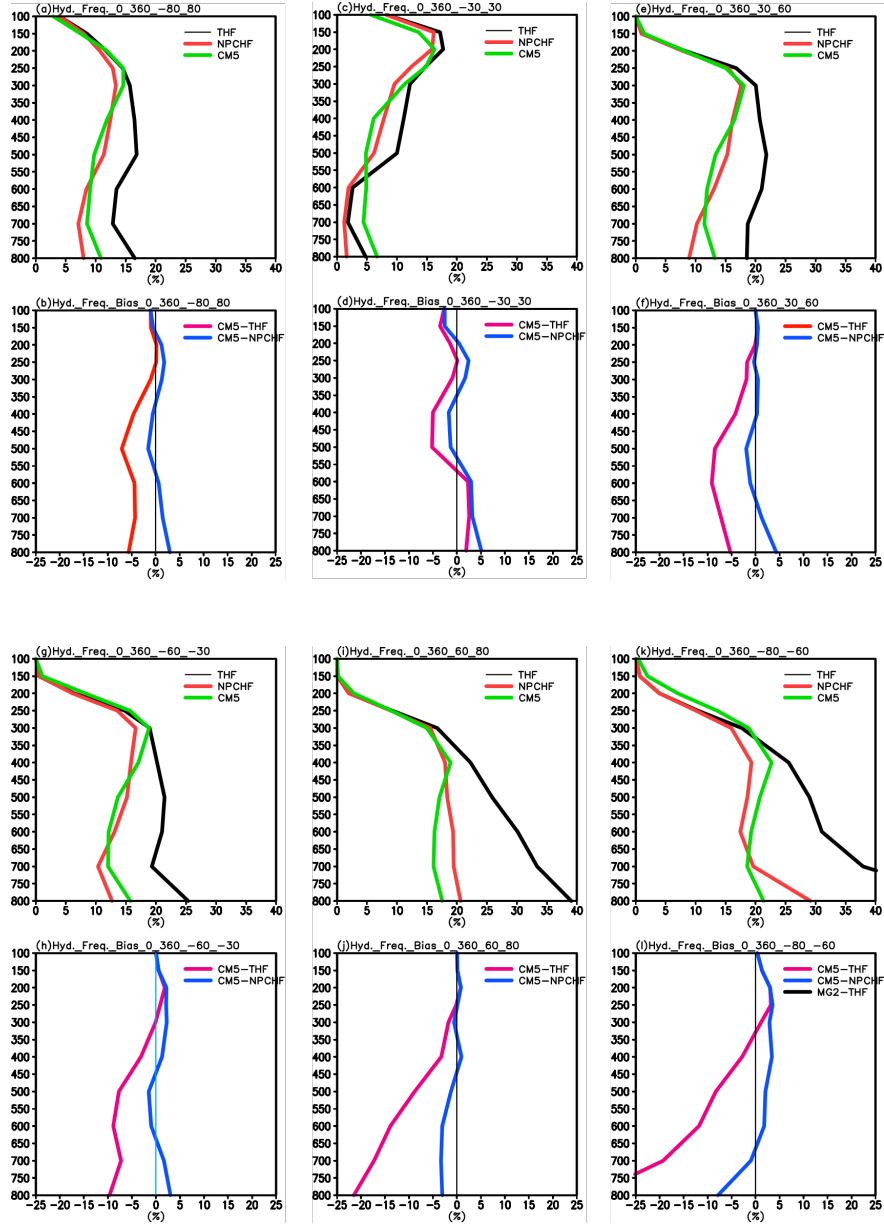
<sup>8</sup>Jet Propulsion Laboratory

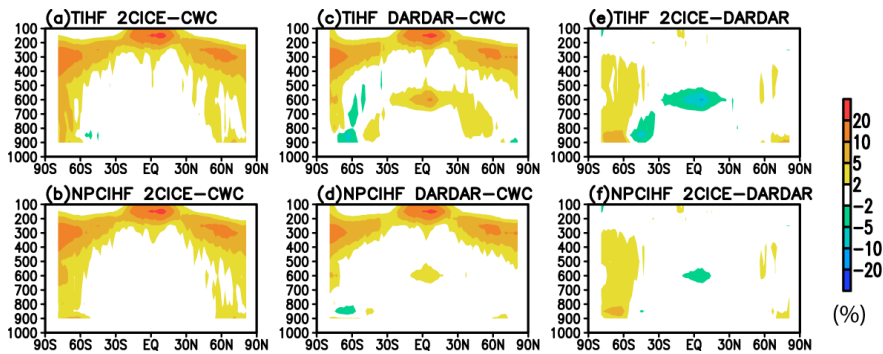
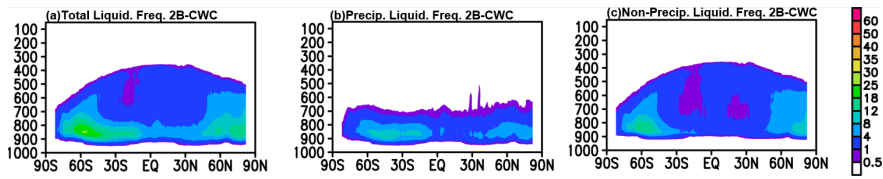
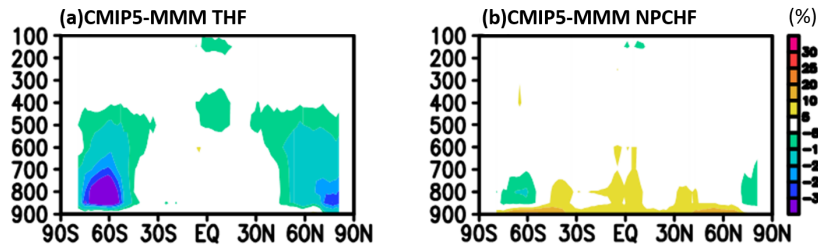
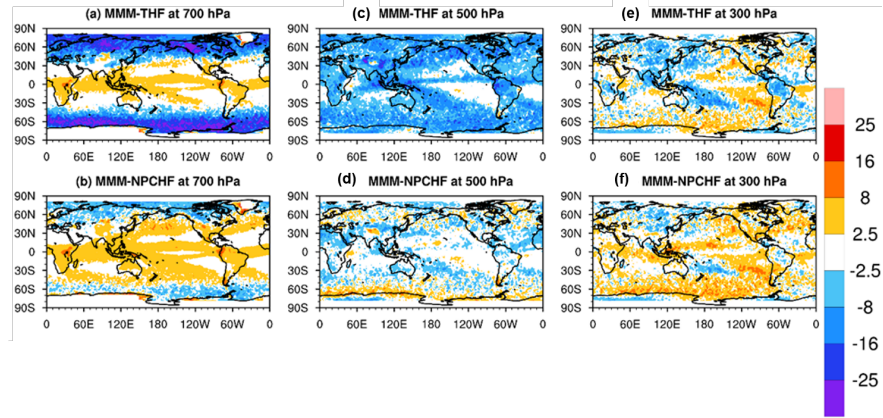
<sup>9</sup>National Taiwan University

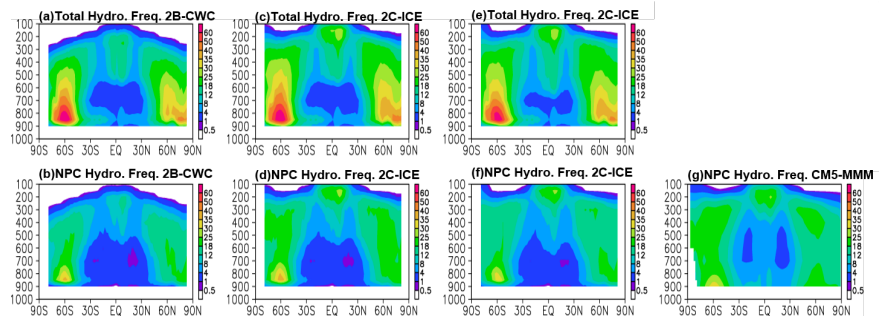
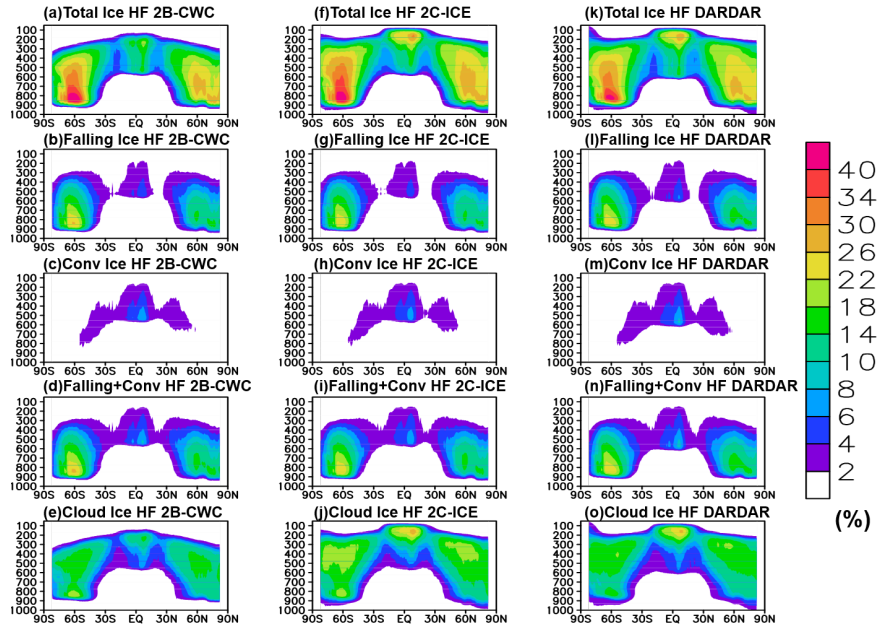
December 20, 2022

## Abstract

This study derives radiatively-active hydrometeors frequencies (HFs) from CloudSat-CALIPSO satellite data to evaluate cloud fraction in present-day simulations by CMIP5 models. Most CMIP5 models do not consider precipitating and/or convective hydrometeors but CESM1-CAM5 in CMIP5 has diagnostic snow and CESM2-CAM6 in CMIP6 has prognostic precipitating ice (snow) included. However, the models do not have snow fraction available for evaluation. Since the satellite-retrieved hydrometeors include the mixtures of floating, precipitating and convective ice and liquid particles, a filtering method is applied to produce estimates of cloud-only HF (or NPCHF) from the total radiatively-active HF (THF), which is the sum of NPCHF, precipitating ice HF and convective HF. The reference HF data for model evaluation include estimates of liquid-phase NPCHF from CloudSat radar-only data (2B-CWC) and ice-phase THF from CloudSat-CALIPSO 2C-ICE combined radar/lidar data. The model evaluation results show that cloud fraction from CMIP5 multi-model mean (MMM) is significantly underestimated (up to 30 %) against the total HF estimates, mainly below the mid-troposphere over the extratropics and in the upper-troposphere over the midlatitude lands and a few tropical convective regions. The CMIP5 cloud fraction biases are reduced dramatically when compared to the cloud-only HF estimates, but the area of overestimates expands from the tropical convective regions to mid-latitudes in the lower and upper troposphere. There is no CMIP5 standard output snow fraction available for comparison against CloudSat-CALIPSO estimate. The implications of these results show that hydrometeors frequency estimates from CloudSat-CALIPSO provide a reference for GCM's cloud fraction from stratiform and convective form.







1  
2 **Radiatively Active Hydrometeors Frequencies from CloudSat-CALIPSO Data for**  
3 **Evaluating Cloud Fraction in Global Climate Models**

4  
5 **Li, Jui-Lin F.<sup>1,2</sup>, \*\*Wei-Liang Lee<sup>3</sup>, Kuan-Man Xu<sup>4</sup>, Yu-Cian Tsai<sup>5</sup>, Jonathon Jiang<sup>1</sup>, Jia-**  
6 **Yuh Yu<sup>5</sup>, Graeme Stephens<sup>1</sup>, Eric Fetzer<sup>1,2</sup>, W-T Chen<sup>6</sup>**

7  
8 *<sup>1</sup>Jet Propulsion Laboratory, California Institute of Technology, Pasadena, CA, USA*

9 *<sup>2</sup>Joint Institute for Regional Earth System Science and Engineering, University of California, Los*  
10 *Angeles, CA, USA*

11 *<sup>3</sup>Research Center for Environmental Changes, Academia Sinica, Taipei, Taiwan*

12 *<sup>4</sup>Science Directorate, NASA Langley Research Center, Hampton, VA, USA*

13 *<sup>5</sup>Department of Atmospheric Sciences, National Central University, Taoyuan City, Taiwan*

14 *<sup>6</sup>Department of Atmospheric Sciences, National Taiwan University, Taipei City, Taiwan*

15  
16 **Submitted to *J. Geophys. Res. Atmos.***

17 ***Jet Propulsion Laboratory/NASA, CalTech***

18  
19 © 2022. All rights reserved.

20 2022

21  
22 **\*\*Corresponding Author: Wei-Liang Lee: [leelupin@gate.sinica.edu.tw](mailto:leelupin@gate.sinica.edu.tw)**

23  
24  
25  
26  
27  
28  
29  
30  
31  
32  
33  
34  
35  
36  
37  
38  
39  
40  
41  
42  
43  
44  
45

**Abstract**

This study derives radiatively-active hydrometeors frequencies (HFs) from CloudSat-CALIPSO satellite data to evaluate cloud fraction in present-day simulations by CMIP5 models. Most CMIP5 models do not consider precipitating and/or convective hydrometeors but CESM1-CAM5 in CMIP5 has diagnostic snow and CESM2-CAM6 in CMIP6 has prognostic precipitating ice (snow) included. However, the models do not have snow fraction available for evaluation. Since the satellite-retrieved hydrometeors include the mixtures of floating, precipitating and convective ice and liquid particles, a filtering method is applied to produce estimates of cloud-only HF (or NPCHF) from the total radiatively-active HF (THF), which is the sum of NPCHF, precipitating ice HF and convective HF. The reference HF data for model evaluation include estimates of liquid-phase NPCHF from CloudSat radar-only data (2B-CWC) and ice-phase THF from CloudSat-CALIPSO 2C-ICE combined radar/lidar data. The model evaluation results show that cloud fraction from CMIP5 multi-model mean (MMM) is significantly underestimated (up to 30 %) against the total HF estimates, mainly below the mid-troposphere over the extratropics and in the upper-troposphere over the midlatitude lands and a few tropical convective regions. The CMIP5 cloud fraction biases are reduced dramatically when compared to the cloud-only HF estimates, but the area of overestimates expands from the tropical convective regions to mid-latitudes in the lower and upper troposphere. There is no CMIP5 standard output snow fraction available for comparison against CloudSat-CALIPSO estimate. The implications of these results show that hydrometeors frequency estimates from CloudSat-CALIPSO provide a reference for GCM's cloud fraction from stratiform and convective form.

46 **The three key points:**

47 **Key point #1:** Deriving non-precipitating and non-convective (cloud only) and total radiatively-  
48 active hydrometeor frequency (HF) from CloudSat-CALIPSO data.

49 **Key point #2:** Cloud fractions from CMIP5 multi-model-mean compare well to cloud-only HF  
50 estimates, implying severely underestimated against total HF estimates.

51 **Key point #3:** Hydrometeors frequency estimates from CloudSat-CALIPSO provides a reference  
52 for GCM's cloud fraction from stratiform and convective form.

53

## 54 **1. Introduction**

55 Both the frequency and mass of radiatively active hydrometeors, including floating cloud  
56 ice and liquid, precipitating hydrometeors (snow), and convective ice and liquid, are important for  
57 atmospheric shortwave (SW) and longwave (LW) radiation computation (Li et al., 2013, 2018;  
58 Waliser et al., 2011; Gettelman et al., 2010; Gettelman and Morrison, 2015; Michibata et al., 2019).  
59 However, most general circulation models (GCMs), such as those participating in the 5<sup>th</sup> phase of  
60 Coupled Model Intercomparison Project (CMIP5) (Taylor et al., 2001; Gleckler et al., 2011), and  
61 the 6<sup>th</sup> phase (CMIP6) (except the CESM2-CAM6 family that considers snow-radiative effects)  
62 only consider the mass and frequency of floating cloud ice and liquid, ignoring radiatively  
63 important precipitating hydrometeor and convective core hydrometeor. Thus, the modeled  
64 atmospheric heating profiles and possibly the global radiation balance may be impacted by the  
65 missing hydrometeors because atmospheric radiation is sensitive to the broader range of  
66 hydrometeors (Li et al., 2012; Waliser et al., 2009). The miscounted or misrepresented mass of  
67 precipitating ice and convective core hydrometeors result in underestimated total ice water content  
68 and path (Li et al., 2012), which are expected to contribute to model biases of radiation budget (Li  
69 et al., 2013). Our previous studies have been focusing on characterizing and diagnosing systematic  
70 biases in the CMIP3/CMIP5/CMIP6 models associated with the precipitating ice radiative effects  
71 as well as the biases in weather models such as the European Centre for Medium-range Weather  
72 Forecast (ECMWF) (Li et al., 2014b). For example, these biases produce underestimated land  
73 surface temperature (Li et al., 2016b), overestimated sea ice concentration (Li et al., 2022) and  
74 have impacts on the modeled sea surface temperatures (Li et al., 2014a, 2016a, b, 2021).

75 While the aforementioned systematic biases contributed by ignoring the precipitating  
76 hydrometeors mass exist in many GCMs, it is essential to evaluate their performance in terms of

77 the frequency (fraction) of radiatively active hydrometeors because it also contributes to  
78 atmospheric radiation in GCMs. However, satellite observations (e.g., CloudSat and CALIPSO)  
79 only provide retrievals of the total water mass for liquid and ice, which is the sum of floating  
80 water/ice and precipitating water/ice in stratiform clouds and convective cores (Li et al., 2012).  
81 Therefore, they are not suitable for direct comparisons with the mass and frequency of non-  
82 precipitating and non-convective hydrometeors produced by most GCMs. To separate the floating  
83 cloud ice from precipitation and convective cores, Chen et al. (2011) and Li et al. (2012) developed  
84 filtering methods to provide (floating) cloud ice water content (CIWC). These concepts and  
85 datasets have been widely employed by the scientific community. For example, Gettelman et al.  
86 (2010) used CIWC to evaluate new ice cloud microphysical approaches for the Community  
87 Atmosphere Model version 5 in the Community Earth System Model version 1 (CESM1-CAM5)  
88 and to develop a new convection scheme with convective cloud ice mass included in CAM5 (Song  
89 et al., 2012). Zhang et al. (2014) investigated ice nucleation in cirrus clouds. The dataset has also  
90 been used to evaluate the IWC representation in the UCLA GCM (Ma et al., 2012), the Weather  
91 Research and Forecasting (WRF) model (Wu et al., 2015), and the Goddard Multiscale Modeling  
92 System (Tao et al., 2009). Another approach is to use satellite simulator software for model  
93 assessment (Bodas-Salcedo et al., 2011), such as using the GCM-Oriented CALIPSO Cloud  
94 Product (CALIPSO-GOCCP) (Cesana et al., 2016), and to evaluate model's cloud phase transition  
95 and low cloud feedback (Cesana et al., 2019). But this approach does not separate the different  
96 types of hydrometeors frequency and might miss the frequency of large particles, which are  
97 detected by CloudSat radar but not by CALIPSO lidar (Cesana et al., 2019).

98           It is noted that the aforementioned studies have focused on the mass and radiative effects  
99 of cloud and precipitating hydrometeors. In this study, we turn our perspective to the occurrence

100 of the radiatively active hydrometeor frequency (HF), which is generally considered equivalent to  
101 the cloud fraction except for sampling cloud fields at a fixed location in time (Clothiaux et al.,  
102 2009; Xu et al., 2012) or on a narrow satellite swath in space such as CloudSat and CALIPSO.  
103 The objective of this study is to provide an observational estimate to evaluate different types of  
104 HF (cloud fraction in model output), including cloud ice, precipitating ice, and cloud liquid, from  
105 the CMIP5 models. Three retrieval algorithms, either using CloudSat radar or CALIPSO lidar or  
106 both, provide global retrievals of ice water content (IWC), including small particles (floating cloud  
107 ice) to larger particles (snow), and liquid water content (LWC), as well as the effective radius (Re)  
108 and the extinction coefficient from the thinnest cirrus (seen only by the lidar) to the thickest ice  
109 cloud (Austin et al., 2001; Hogan et al., 2006; Delanoë and Hogan, 2008, 2010; Macc et al., 2009;  
110 Young and Vaughan, 2009; Sassen et al., 2009; Deng et al., 2010; Stein et al., 2011). In this study,  
111 we use cloud liquid HF from CloudSat-only 2B-CWC-RO5 product (Austin et al., 2009; Li et al.,  
112 2018), combined with CloudSat-CALIPSO ice water products from 2C-ICE (Deng et al., 2010,  
113 2013) and DARDAR (raDAR/liDAR) (Hogan, 2006; Delanoë and Hogan, 2008, 2010) for  
114 obtaining the total HF (THF), non-precipitating and non-convective HF (NPCHF), precipitating  
115 ice HF (PIHF), and convective HF (CHF), so that a robust and meaningful observational HF  
116 estimate can be made for model evaluations.

117 In Section 2, we describe the observational resources for the estimated hydrometeor  
118 frequency from CloudSat-CALIPSO data, the separation of different types of hydrometeor  
119 frequencies and the cloud fractions in model simulations. In Section 3, we discuss the results with  
120 a summary and conclusions drawn in Section 4.

121

## 122 **2. Reference Datasets, Separation of Hydrometeors Frequency and Model output**

### 123 **2.1 Hydrometeors Frequency Reference Datasets**

124 We generate five types of HF, based on the “FLAG” method developed in Waliser et al.  
125 (2009) and Li et al. (2012, 2018), for non-precipitating and non-convective floating cloud ice  
126 (FIHF) and cloud liquid (FLHF), convective ice (CIHF) and convective liquid (CLHF), and  
127 precipitating ice (PIHF) associated with their respective masses, using CloudSat-CALIPSO  
128 measurements including 2B-CWC, 2C-ICE, and DARDAR datasets. The sum of FIHF and FLHF  
129 is also called, interchangeably, non-precipitating and non-convective HF (NPCHF) or cloud-only  
130 HF. These three datasets cover the period of January 2007 to December 2010.

131 (a) *2B-CWC-RO5* (Austin et al., 2001, 2009) is a CloudSat-only product that provides  
132 estimates of the hydrometeor content from measured radar reflectivity to constrain the  
133 retrieved mass of both liquid and ice phases for all heights.

134 (b) *DARDAR* (raDAR/liDAR) (Hogan, 2006; Delanoë and Hogan, 2008, 2010) is a synergistic  
135 ice cloud retrieval product derived from the combination of the CloudSat radar and  
136 CALIPSO lidar using a variational method for retrieving profiles of the extinction  
137 coefficient, IWC, and equivalent radius ( $R_e$ ) of the ice cloud (Brown and Francis, 1995;  
138 Francis et al., 1998; Delanoë et al., 2011; Stein et al., 2011; Delanoë and Hogan, 2010).

139 (c) *2C-ICE* (Deng et al., 2010) provides ice cloud retrieval also derived from the combination  
140 of the CloudSat radar and CALIPSO lidar. While using the same satellite input, *2C-ICE* is  
141 different from *DARDAR* in many ways, such as the vertical resolution, treatments of  
142 multiple scattering and backscattering, and assumptions of the particle size distribution.  
143 Readers desiring a more in-depth description of the *2C-ICE* algorithm should refer to Deng  
144 et al. (2010, 2013) for details.

## 145 **2.2 Separation of Hydrometeors Frequency**

146           There are two essential aspects regarding the compatibility of the hydrometeor mass and  
147 frequency between model and observation. First, CALIPSO measurements used in the DARDAR  
148 and 2C-ICE products have more sensitivity to small and thin cirrus clouds that might make very  
149 little contribution to the total ice mass and water content of clouds but could play an important role  
150 in the radiation budget (Liou, 1986, 2002; Sassen, 2003; Schumann, 2002, 2009). Second, more  
151 importantly, all three products, to first order, represent the total tropospheric ice/liquid, including  
152 “floating” cloud ice/liquid and the precipitating ice (snow) with variable sizes and terminal  
153 velocities as the combined measurements are sensitive to a wide range of particle sizes. The  
154 particle sizes, including those of particles associated with convective clouds, are generally not  
155 included as prognostic variables in all current GCMs (e.g., Li et al., 2012; Waliser et al., 2009).  
156 Furthermore, it is generally assumed that convective core areas are small relative to a grid box in  
157 a typical GCM grid box size larger than a few hundred km<sup>2</sup>. Thus, its contribution to HF and mass  
158 is not very large. Even if it is either prognostically or diagnostically determined, the relative  
159 contribution does not change. However, as the resolution in the most current state-of-the-art GCMs  
160 become higher, with grid box size smaller than 100 km<sup>2</sup> to tens of km<sup>2</sup>, the contribution of HF and  
161 mass of the convective cores should be considered.

162           In this study, we use the “FLAG-method,” following Waliser et al. (2009) and Li et al.  
163 (2012), to distinguish HFs associated with clouds with ice/liquid mass from HFs associated with  
164 precipitation and convection. This method is summarized as follows. To achieve the separation of  
165 HFs of different types, we exclude all the retrievals in any profile that are flagged as precipitating  
166 at the surface and any retrieval within the profile whose cloud type is classified as “deep  
167 convection” or “cumulus” (from CloudSat 2B-CLDCLASS dataset; Sassen and Wang, 2008). The  
168 remaining profiles are associated with clouds with floating ice/liquid mass. Their frequencies are

169 called either floating ice HF (FIHF) or floating liquid HF (FLHF), depending on the cloud phase.  
170 The frequencies of the excluded profiles associated with precipitation are called precipitating ice  
171 HF (PIHF) while precipitating liquid (rain) is not important for radiative calculation, which will  
172 not be discussed. The frequencies of the excluded profiles associated with convection are called  
173 either convective ice HF (CIHF) or convective liquid HF (CLHF), depending upon the cloud  
174 phase. The total ice hydrometeor frequency (TIHF) is the sum of FIHF, PIHF and CIHF while the  
175 total liquid HF (TLHF) is the sum of FLHF and CLHF. This methodology was used for estimating  
176 CIWP/CIWC used for CMIP3 model-data comparisons (e.g., Li et al., 2012; Waliser et al., 2009)  
177 and for model cloud parameterizations improvements in CAM5 (Gettelman et al., 2010; Song et  
178 al., 2011), as well as other applications mentioned in the introduction.

179         The caveat of the aforementioned HF separation method that we need to keep in mind is  
180 that it is impossible to completely separate floating/cloudy forms from precipitating forms, as they  
181 coexist at some height intervals. Specific retrievals of this sort will require co-located vertical  
182 velocity information, such as from a Doppler radar capability and/or a multiple frequency radar,  
183 to better characterize particle sizes that are not available yet. Thus, it is beyond the scope of this  
184 study.

185 **2.3 Cloud Fraction in GCMs**

186         The protocol output of cloud fraction from all CMIP5 models only includes “cloud only”  
187 fraction, which is equivalent to non-precipitating and non-convective HF (NPCHF) from  
188 observational estimate outlined above. Some CMIP5 models do consider convective ice and/or  
189 diagnostic precipitating ice (snow) hydrometeors such as CESM1-CAM5, however, the model  
190 does not have snow fraction output available. The CMIP5 simulations used in this study are listed  
191 in Table A1, which provides an outline of cloud microphysics parameterizations used in each

192 model. The historical simulation, which used observed 20<sup>th</sup>-century greenhouse gases, ozone,  
193 aerosol, and solar forcing, is analyzed. The period used for the long-term mean is 1970-2005, and  
194 if a model provided multiple members of simulations, only one of them was chosen for this  
195 evaluation. For the purposes of comparison, both the GCM and observational datasets are re-  
196 gridded into a common horizontal grid of 2° latitude by 2° longitude. Figure 1h shows the zonally-  
197 averaged cloud fraction (ice+liquid) distribution from the CMIP5 multi-model-mean (MMM).

198 In addition to the CMIP5 model output, we also discuss the CESM2-CAM6 model output.  
199 The CAM6 implements a new prognostic cloud microphysics scheme for cloud ice, liquid,  
200 precipitating ice, and rain (Gettelman and Morrison, 2015; MG2). However, the model does not  
201 provide comparable output for snow fraction for comparisons.

## 202 **3. Results**

### 203 **3.1 Observational Estimates of Hydrometeor Frequencies**

204 To account for the observational uncertainty of HFs, we produce three different estimates  
205 of HFs from 2B-CWC, 2C-ICE, and DARDAR datasets in this study. Shown in Figure 2 are the  
206 zonally-averaged HFs determined by nonzero radar/lidar reflectivity from CloudSat/CALIPSO  
207 data with the classification of precipitation and convection based on surface precipitation and  
208 convective cloud flags, respectively. These are averaged from 2007 to 2010 in time. These HFs  
209 include total ice HF (TIHF; panels a, f and k), which is the sum of precipitating ice HF (PIHF;  
210 panels b, g and l), convective ice HF (CIHF; panels c, h and m), and floating cloud ice frequency  
211 (FIHF; panels e, j and o). Panels d, i and n show the sum of PIHF and CIHF. Figures 2a-2g are for  
212 2B-CWC, Figures 2f—2j are for 2C-ICE, and Figures 2k—2o are for DARDAR.

213 Overall, the precipitating ice HF dominates the total ice HF; i.e., PIHF is 22—26% below  
214 400 hPa, compared to 30—40% of TIHF over the mid-latitudes of both hemispheres (Figures 2b,

215 2g, 2l). The convective ice HF (CIHF) contributes about 6—8% between 350—500 hPa from the  
216 tropical convective zones (Figures 2c, 2h, 2m). Cloud-only ice HF (FIHF) (Figures 2e, 2j, 2o)  
217 represents 10—26% contribution, which is smaller than the PIHF over the mid-latitudes. But FIHF  
218 is larger in the upper troposphere over the tropics and midlatitudes. This is especially true for 2C-  
219 ICE and DARDAR datasets because thin ice clouds can be detected by CALIPSO lidar, but not by  
220 CloudSat radar (2B-CWC). Nevertheless, the differences in PIHF between 2C-ICE and DARDAR,  
221 as discussed below, are much smaller, compared to their differences with 2B-CWC.

222 To see the differences between the three datasets, the total ice HF and floating ice HF  
223 differences are calculated between 2C-ICE and 2B-CWF (Figures 3a and 3b), between DARDAR  
224 and 2B-CWC (Figures 3c and 3d) and between 2C-ICE and DARDAR (Figures 3e and 3f). It is  
225 evident that TIHF (Figure 3a and 3c) and FIHF (Figure 3b and 3d) estimates from the 2C-ICE and  
226 DARDAR datasets are much larger above 300-hPa levels over the tropics and above 500-hPa  
227 levels over the mid-latitudes than the radar-only 2B-CWC data. This is due to the fact that most  
228 small ice particles in cirrus clouds detected by CALIPSO lidar (2C-ICE and DARDAR) are  
229 invisible to CloudSat radar (2B-CWC), resulting in minimal amounts of HF in 2B-CWC over the  
230 upper troposphere. Since the TIHF and FIHF differences between 2C-ICE and DARDAR datasets  
231 (Figure 3e and 3f) are only ~2%, we will use 2C-ICE as our reference to compare the observed  
232 frozen hydrometeors frequencies (i.e., FIHF, PIHF and TIHF) with CMIP5 models in this study.  
233 As discussed later, the differences in HFs between models and observational estimates are much  
234 larger than 2%.

235 We also generate estimates of total liquid HF (TLHF), precipitating liquid HF (PLHF),  
236 and floating cloud liquid HF (FLHF) based on 2B-CWC dataset, which are shown in Figures 4a-  
237 c. They, as expected, have large values in the lower troposphere but not detected below ~900 hPa

238 due to ground clutter effects of CloudSat radar. The maximum FLHF occurs between 800—900  
239 hPa in the midlatitudes while the smallest FLHP occurs above ~800 hPa in the subtropics of both  
240 hemispheres due to large-scale subsidence. Note that the precipitating liquid (rain) is not  
241 radiatively active due to its large particle size. Therefore, only FLHF and convective liquid HF are  
242 considered as parts of the total HF in this study.

243 To get the total HF (THF), we add float liquid HF (FLHF) to total ice HF (TIHF). We also  
244 add FLHF to float ice HF (FIHF) to produce the estimate of non-precipitating and non-convective  
245 HF (NPCHF), total floating HF (TFHF) or cloud-only HF. The zonally-averaged annual mean  
246 THF and NPCHF are shown for 2B-CWC (Figure 1a, b), for 2C-ICE (Figure 1c, d), and DARDAR  
247 (Figure 1e, f), respectively. These estimated HFs can be used as references for evaluating cloud  
248 fractions in GCMs. The comparisons with GCMs are shown in the following sections.

### 249 ***3.2 Comparison of zonally-averaged hydrometeor frequency***

250 Figure 5 shows the differences of CMIP5-MMM cloud fractions from the combined THF  
251 and NPCHF estimates of frozen HFs from Cloudsat-CALIPSO 2C-ICE and floating liquid HF  
252 from 2B-CWC, which are used as the reference data. Differences for CMIP5-MMM from other  
253 reference data are shown in Figure A1. The zonally-averaged CMIP5-MMM cloud fraction is  
254 substantially smaller than the estimated THF by up to 20—60% over the southern and northern  
255 hemisphere mid- and high-latitudes, as shown in Figure 5a. On the contrary, it is reasonably well  
256 described compared to the estimated NPCHF with biases within 5% (Figure 5b). The excessive  
257 cloud fraction in the mid-troposphere of the tropics might be due to the uncertainty of the  
258 missing/undetected hydrometeors from CloudSat-CALIPSO caused by the strong attenuation of  
259 radar/lidar signals under thick convective cloud regions.

260

261

### 262 *3.3 Comparison of regionally averaged profiles of hydrometeor frequency*

263 Figure 6 shows the profiles of regional area averages of CMIP5-MMM cloud fractions  
264 against the estimated NPCHF and THFs for the globe [panels (a) and (b): 80°S—80°N], tropics  
265 [panels (c) and (d): 30°S—30°N], northern hemisphere (NH) mid-latitudes [panels (e) and (f):  
266 30°N—60°N] and high-latitudes belts [panels (i) and (j): 60°N—80°N], and southern hemisphere  
267 (SH) mid-latitudes [panels (g) and (h): 30°S—60°S] and high-latitudes belts [panel (k) and (l):  
268 60°S—80°S).

269 In general, the mean cloud fractions from CMIP5-MMM over all the above-mentioned  
270 regions agree well to the estimated cloud-only HF (NPCHF) with biases within 5%, as shown in  
271 the lower panels of Figure 6. When compared to the estimated THF, the mean CMIP5-MMM cloud  
272 fractions are underestimated below 300 hPa for all the above-mentioned regions because CMIP5  
273 models do not have precipitating ice and convective cloud hydrometeors included in cloud  
274 fractions. That is, precipitating ice and convective cores do not impact radiative calculation in  
275 these models. The maximum magnitudes of underestimated CMIP5 cloud fractions could reach up  
276 to 20—25% for mid- and high-latitudes over both hemispheres (Figures 6g, 6h, 6i, 6j, 6k, 6l),  
277 mainly due to the lack of precipitating ice cloud fractions. In reality, they are contributed by mid-  
278 and high-latitudes storms and stratiform precipitating ice over the polar regions.

279

### 280 *3.4. Comparison of horizontal distributions of hydrometeor frequency*

281 Figure 7 shows the CMIP5-MMM cloud fraction biases at 700 hPa, 500 hPa, and 300 hPa  
282 against the estimated THF (Figures 7a, 7d and 7g) and NPCHF (Figures 7b, 7e and 7h). As shown  
283 in Figure 7a, at 700 hPa, it is evident that CMIP5-MMM substantially underestimates the THF

284 north of 40°N and south of 40°S over storm tracks and the Arctic and Antarctic regions due to the  
285 lack of precipitating ice in CMIP5 models. The slightly overestimated CMIP5-MMM cloud  
286 fractions over convective zones might be due to the strong attenuation of radar signals below thick  
287 convective clouds that are not detected by the CloudSat radar. Compared to the estimated cloud-  
288 only HF, CMIP5-MMM cloud fractions are overestimated over the convective zones and storm  
289 track regions but still underestimated in the polar regions, as shown in Figure 7b. In general,  
290 CMIP5-MMM cloud fractions at 700 hPa are very close to the estimated NPCHF with magnitude  
291 differences less than 8%.

292 At 500 hPa, the CMIP5-MMM cloud fractions are generally underestimated over mid- and  
293 high-latitudes storm tracks and over convectively active regions such as the ITCZ, SPCZ, and  
294 warm pool due to the lack of stratiform precipitating ice and convective ice, compared to the  
295 estimated THF, as shown in Figure 7d. In contrast, they show very small biases against the  
296 estimated NPCHF with biases less than 2.5% (Figure 7e).

297 At 300 hPa, the CMIP5-MMM cloud fractions are slightly underestimated (-2.5 — -8%)  
298 against the estimated THF (Figure 7g). The largest underestimates occur in places where  
299 precipitating ice HF is expected to be large; for example, over the storm track in the North Pacific,  
300 midlatitude lands and convectively-active regions over the SPCZ and warm pool. Interestingly,  
301 the CMIP5-MMM cloud fractions are larger than the estimated THF over the South Pacific trade-  
302 wind regions and the Southern Ocean, indicating that the CMIP5 models simulate excessive high  
303 clouds over these regions (Figure 7g and 7h). This feature over the trade-wind regions is not shown  
304 over the zonally-averaged profiles (Figures 5a, 5b and 6) due to the cancellation associated with  
305 underestimates over the SPCZ. In our previous study (Li et al., 2021), we attributed this excessive  
306 cloud fraction in CMIP5-MMM to hydrometeor-radiation-circulation coupling biases caused by

307 the lack of precipitating ice radiative effects over the convective regions, leading to weaker surface  
308 wind stress, weaker trade-winds speed (effectively moist and warm advection into the region) and  
309 warmer SSTs, consequently producing high-level convective clouds over the trade-wind regions.  
310 It seems that the southeast Pacific trade-wind region does not have clouds at 300 hPa or not as  
311 much as those in CMIP5-MMM.

312

#### 313 **4. Summary and Conclusions**

314 The radiative properties of hydrometeors that are input to radiative calculation in GCMs  
315 include the mass and hydrometeors occurrence frequency. The purpose of this study is to make  
316 judicious comparisons and evaluations of the GCM representations of cloud fraction against the  
317 satellite observations of radiatively-active hydrometeor frequencies, which are inherently the  
318 combination of cloud-only ice/liquid and precipitating ice (snow). We employ a set of satellite  
319 observations of hydrometeors, including 2B-CWC-RO5 from the CloudSat radar for cloud liquid  
320 frequency and 2C-ICE and DARDAR from the combined CloudSat radar and CALIPSO lidar  
321 retrievals for frequency of cloud ice and precipitating ice (snow+graupel+hail). Then the FLAG  
322 method developed by Li et al. (2012) is used to categorize different types of hydrometeors  
323 frequency for floating cloud liquid/ice, precipitating ice, and convective liquid/ice.

324 We examined the annual-mean zonally averaged hydrometeor frequency estimates from  
325 the 2B-CWC, 2C-ICE, and DARDAR datasets. The HF derived from the 2B-CWC radar only data  
326 does not detect small ice particles such as suspended thin cirrus while it can be captured by the  
327 CALIPSO lidar used in the 2C-ICE and DARDAR datasets. It is noted that the differences in  
328 frozen hydrometeors and total hydrometeor frequencies are trivial between 2C-ICE and  
329 DARDAR. Therefore, we choose ice HF of 2C-ICE and liquid HF from 2B-CWC as a reference

330 for evaluating model simulation of cloud fraction. The filtered frequency of non-precipitating and  
331 non-convective hydrometeors (NPCHF, also called cloud-only HF) and total HF (THF), which is  
332 the sum of NPCHF, convective liquid/ice and precipitating ice (snow) HFs, can be utilized for a  
333 sensible “apple to apple” comparison within the limitation of measurement accuracy for models  
334 that produce either cloud-only cloud fraction (CMIP5 models) or cloud fraction with snow  
335 considered for computing the associated radiative effects in GCMs (such as in CESM2-CAM6 in  
336 CMIP6), respectively. Note that the precipitating liquid (rain) is not radiatively active in all current  
337 GCMs except in new version of GISS-E3 (Li et al., 2022). However, there is no snow fraction  
338 output available in CESM2-CAM6 for model-data comparison. In this study, we can only do the  
339 model-data evaluation for cloud-only liquid and ice frequency (fraction) in the CMIP5 models.

340 We evaluated zonally-averaged cloud (only) fraction from multi-model-mean (MMM) of  
341 CMIP5 historical simulations during 1970—2005 against the estimated THF and cloud-only HF.  
342 The performance of simulated CMIP5-MMM cloud fraction is extremely well in comparison to  
343 the estimated cloud-only HF with biases within 5%, except for some overestimates over the  
344 midlatitudes of both hemispheres, probably due to the attenuation of radar/lidar signals by thick  
345 clouds. When compared to the total HF (THF), CMIP5-MMM cloud fraction is underestimated  
346 with biases more than 30% magnitudes over the mid- to high-latitudes and the deep tropics below  
347 700 hPa due to the lack of precipitating ice in the CMIP5 models. The underestimates are  
348 drastically reduced over the high latitudes, compared to CMIP5-MMM.

349 We further examined the hydrometeor frequency of the CMIP5 in terms of regionally area-  
350 averaged profiles of CMIP5-MMM cloud fraction against the estimated cloud-only and total HF  
351 for global, tropical, and mid- and high-latitudes belts. We found that the performance of CMIP5-  
352 MMM is very good for all regions against the estimated cloud-only HF profiles, agreeing with

353 each other with biases within 5%. However, compared to the estimated total HF (THF) profiles,  
354 all regionally-averaged profiles of CMIP5-MMM HF are significantly underestimated (20—25%)  
355 because the CMIP5 models do not have precipitating ice and convective hydrometeors, in  
356 particular, over the mid- and high-latitude belts and stratiform precipitating ice over the polar  
357 latitudes.

358 To better understand the characteristics of cloud fraction biases, we examined the spatial  
359 patterns of CMIP5-MMM cloud fraction biases against the estimated cloud-only and total HFs at  
360 700 hPa, 500 hPa, and 300 hPa. Compared to the total HF, the CMIP5-MMM cloud fraction at  
361 700 hPa is underestimated by as large as 25% north of 40°N and south of 40°S, including storm  
362 tracks and the Arctic and Antarctic regions, due to the lack of precipitating ice in CMIP5-MMM.  
363 It is also underestimated everywhere at 500 hPa with smaller biases than at 700 hPa and slightly  
364 underestimated over the northern hemisphere midlatitudes and SPCZ. On the other hand, CMIP5-  
365 MMM cloud fraction is overestimated over the tropical convective zones, probably caused by  
366 attenuation of radar signals below thick convective clouds. Compared to the estimated cloud-only  
367 HF at 700 hPa, the CMIP5-MMM cloud fraction biases are reduced significantly over the polar  
368 regions and it is also reduced everywhere at 500 hPa with biases less than 2.5%, but areas with  
369 overestimates increase from the tropical convective regions to the middle latitudes at 700 hPa and  
370 to the Southern Ocean at 300 hPa. It is also noted that at 300 hPa, CMIP5-MMM has overestimated  
371 cloud fractions (2.5 — 16%) over the southern Pacific trade-wind regions, indicating that the  
372 CMIP5 models tend to simulate too many high clouds over these regions, which might be related  
373 to the bias of cloud-radiation-dynamics coupling produced by the lack of precipitating ice radiative  
374 effects in the convective regions reported in Li et al. (2021).

375           In summary, while most of the CMIP5 models do not consider radiatively active  
376 precipitating ice and/or convective hydrometeor, we provide estimates of HF for cloud-only  
377 (NPCHF) so that a robust estimated HF can be used for model evaluation within the limitations of  
378 measurement accuracy, which can vary with cloud and precipitating types that cannot be qualified  
379 in this study. The results show that the HF is significantly underestimated in CMIP5 MMM (up to  
380 30 %) against the observational total HF (THF), while the CMIP5 models simulate HF quite well  
381 against observational cloud-only HF. The implications of these results on model representations  
382 of cloud fraction should include radiatively active precipitating ice and convective hydrometeor  
383 types besides the cloud-only type to have a complete model-data comparison for cloud and  
384 precipitating ice fraction.

385

386

387 **Acknowledgments**

388 The research was carried out at the Jet Propulsion Laboratory, California Institute of Technology,  
389 under a contract with the National Aeronautics and Space Administration (80NM0018D0004).  
390 This work has been supported primarily by NASA MAP project and in part by the NASA  
391 CloudSat, obs4MIPs, and NASA Making Earth System Data Records for Use in Research  
392 Environments (MEaSUREs) programs. WLL has been supported by the Ministry of Science and  
393 Technology of Taiwan under the contract MOST 110-2111-M-001-008.

394 The availability of vertically-resolved cloud hydrometeor profiles 2C-ICE (Deng et al., 2010,  
395 2013) is derived from *CloudSat*-CALIPSO (Stephens et al., 2008; Austin et al., 2009;  
396 <http://www.cloudsat.cira.colostate.edu/>).

397

398

399

400

401

402

403

404

405

406 **REFERENCES**

- 407 Austin, R., and G. L. Stephens (2001), Retrieval of stratus cloud microphysical parameters using  
408 millimeter-wave radar and visible optical depth in preparation for Cloudsat: 1. Algorithm  
409 formulation, *J. Geophys. Res.*, 106, 28,233– 28,242.
- 410 Austin, R. T., A. J. Heymsfield, and G. L. Stephens (2009), Retrieval of ice cloud microphysical  
411 parameters using the CloudSat millimeter-wave radar and temperature, *J. Geophys.*  
412 *Res.*, 114, D00A23, doi:10.1029/2008JD010049.
- 413 Bodas-Salcedo, A., M. J. Webb, S. Bony, H. Chepfer, J.-L. Dufresne, S. A. Klein, Y. Zhang, R.  
414 Marchand, J. M. Haynes, R. Pincus, and V.O. John, (2011), COSP: Satellite simulation  
415 software for model assessment. *Bull. Amer. Meteor. Soc.*, doi: 10.1175/2011BAMS2856.1
- 416 Brown, P. R. A., and P. N. Francis (1995), Improved measurements of the ice water content in  
417 cirrus using a total-water probe, *J. Atmos. Oceanic Technol.*, 12, 410–414,  
418 doi:10.1175/1520-0426(1995)012<0410: IMOTIW>2.0.CO;2.
- 419 Cesana, G., Del Genio, A. D., Ackerman, A. S., Kelley, M., Elsaesser, G., Fridlind, A. M., et al.  
420 (2019). Evaluating models' response of tropical low clouds to SST forcings using  
421 CALIPSO observations. *Atmospheric Chemistry and Physics*, 19(5), 2813–2832.  
422 <https://doi.org/10.5194/acp-19-2813-2019>.
- 423 Cesana, G., Chepfer, H., Winker, D., Getzewich, B., Cai, X., Jourdan, O., Mioche, G., Okamoto,  
424 H., Hagihara, Y., Noel, V., and Reverdy, M.: Using in situ airborne measurements to  
425 evaluate three cloud phase products derived from CALIPSO: CALIPSO Cloud Phase  
426 Validation, *J. Geophys. Res.-Atmos.*, 121, 5788–  
427 5808, <https://doi.org/10.1002/2015JD024334>, 2016.

428 Chen, W.-T. Chen, C. P. Woods, J.-L. F. Li, D. E. Waliser, J.-D. Chern, W.-K. Tao, J. H. Jiang,  
429 and A. M. Tompkins (2011), Partitioning CloudSat Ice Water Content for Comparison with  
430 Upper-Tropospheric Ice in Global Atmospheric Models, *J. Geophys. Res.*,doi:10.1029/2010JD015179.  
431

432 Clothiaux, E. E., Moran, K. P., Martner, B. E., Ackerman, T. P., Mace, G. G., Uttal, T., Mather, J.  
433 H., Widener, K. B., Miller, M. A. and Rodriguez, D. J., (1999), The Atmospheric Radiation  
434 Measurement program cloud radars: Operational modes. *J. Atmos. Oceanic Tech.*, 16, 819–  
435 827.

436 Delanoë, J., and R. J. Hogan (2008), A variational scheme for retrieving ice cloud properties from  
437 combined radar, lidar, and infrared radiometer, *J. Geophys. Res.*, 113, D07204,  
438 doi:10.1029/2007JD009000.

439 Delanoë, J., and R. J. Hogan (2010), Combined CloudSat-CALIPSO-MODIS retrievals of the  
440 properties of ice clouds, *J. Geophys. Res.*, 115, D00H29, doi:10.1029/2009JD012346.

441 Del Genio, A. D., M.-S. Yao, W. Kovari, and K. K.-W. Lo (1996), A prognostic cloud water  
442 parameterization for global climate models, *J. Climate*, 9(2), 270–304, doi:10.1175/1520-  
443 0442(1996)009<0270:APCWPF>2.0.CO;2.

444 Deng, M., G. G. Mace, Z. Wang, and H. Okamoto (2010), Tropical Composition, Cloud and  
445 Climate Coupling Experiment validation for cirrus cloud profiling retrieval using CloudSat  
446 radar and CALIPSO lidar, *J. Geophys. Res.*, 115, D00J15, doi:10.1029/2009JD013104.

447 Deng, M., G. G. Mace, Z. Wang, and R. P. Lawson (2013), Evaluation of several A-Train ice cloud  
448 retrieval products with in situ measurements collected during the SPARTICUS  
449 campaign, *J. Appl. Meteor. Climatol.*, 52, 1014–1030. doi: [10.1175/JAMC-D-12-054.1](https://doi.org/10.1175/JAMC-D-12-054.1).

450 Francis, P. N., P. Hignett, and A. Macke (1998), The retrieval of cirrus cloud properties from  
451 aircraft multi-spectral reflectance measurements during EUCREX'93, *Q. J. R. Meteorol.*  
452 *Soc.*, 124, 1273– 1291.

453 Gettelman, A., X. Liu, S. J. Ghan, H. Morrison, S. Park, A. J. Conley, S. A. Klein, J. Boyle, D. L.  
454 Mitchell, J.-L. F. Li, (2010), Global simulations of ice nucleation and ice supersaturation  
455 with an improved cloud scheme in the Community Atmosphere Model. *J. Geophys. Res.*,  
456 115, D18216, doi:10.1029/2009JD013797.

457 Gettelman, A., and H. Morrison (2015), Advanced two-moment bulk microphysics for global  
458 models. Part I: Off-line tests and comparison with other schemes. *J. Climate*, 28(3), 1268–  
459 1287, doi:10.1175/JCLI-D-14-00102.1.

460 Gleckler, P. R. Ferraro, D. E. Waliser (2011), Better use of satellite data in evaluating climate  
461 models contributing to CMIP and assessed by IPCC, Meeting Summary, EOS, Vol. 92,  
462 No. 20, 17 May 2011.

463 Hogan, R. J. (2006), Fast approximate calculation of multiply scattered lidar returns, *Appl. Opt.*,  
464 45, 5984–5992.

465 Hourdin F., I. and coauthors, (2006), The LMDZ4 general circulation model : climate performance  
466 and sensitivity to parametrized physics with emphasis on tropical convection. *Climate*  
467 *Dynamics*, 19(15) :3445-3482, DOI : 10.1007/s00382-006-0158-0.

468 Le Treut, H., and Z. X. Li, (1991), Sensitivity of an atmospheric general circulation model to  
469 prescribed SST changes: Feedback effects associated with the simulation of cloud optical  
470 properties. *Climate Dyn.*, 5, 175–187.

471 Li, J.-L. F., Gregory V Cesana, Kuan-Man Xu, Mark Richardson, Hanii Takahashi, J. Jiang,  
472 (2022), Comparisons of Simulated Radiation, Surface Wind Stress and SST Fields over  
473 Tropical Pacific by the GISS CMIP6 Versions of Global Climate Models with  
474 Observations, *Environ. Res. Commun.*, IOP, accepted.

475 Li, J.-L. F., and co-authors, (2022), Observational Evaluation of Global Climate Model  
476 Simulations of Arctic Sea Ice Pertaining to the Radiative Effects of Frozen Hydrometeors,  
477 *Environ. Res. Commun.* Volume 4, Number 2, 4 025008.

478 Li, J.-L. F., K.-M. Xu, Wei-Liang Lee, J. H. Jiang, Eric Fetzer, Graeme Stephens, Jia-Yuh Yu, and  
479 Yi-Hui Wang, 2021: Changes of south-central Pacific large-scale environment associated  
480 with hydrometeors-radiation-circulation interactions in a coupled GCM. *J. Geophys. Res.*,  
481 *125*, DOI:10.1029/2021JD034973.

482 Li, J.-L.F., Seungwon Lee, Hsi-Yen Ma, G. Stephens, and Bin Guan, (2018), Assessment of the  
483 Cloud Liquid Water from Climate Models and Reanalyses using Satellite Observations,  
484 *Terrestrial Atmospheric and Oceanic Sciences*, DOI: 10.3319/TAO.2018.07.04.01.

485 Li, J.-L. F., W.-L. Lee, J.-Y. Yu, G. Hulley, E. Fetzer, Y.-C. Chen, and Y.-H. Wang (2016b), The  
486 impacts of precipitating hydrometeors radiative effects on land surface temperature in  
487 contemporary GCMs using satellite observations, *J. Geophys. Res. Atmos.*, *120*,  
488 doi:10.1002/2015JD023776.

489 Li, J.-L. F., W.-L. Lee, Tong Lee, Eric Fetzer, Jia-Yuh Yu, (2016a), The Impacts of Cloud Snow Radiative  
490 Effects on Pacific Oceans Surface Heat Fluxes, Surface Wind Stress, and Ocean Temperatures in  
491 Coupled GCM Simulations, *J. Geophys. Res. Atmos.*, *120*, DOI: 10.1002/2014JD022538.

492 Li, J.-L. F., R. M. Forbes, D. E. Waliser, G. Stephens, S. W. Lee, (2014b), Characterizing the impacts of  
493 precipitating snow hydrometeors in the radiation using the ECMWF IFS global model, *J. Geophys.*  
494 *Res. Atmos.*, 119, doi:10.1002/2014JD021450.

495 Li, J.-L. F., W.-L. Lee, D. E. Waliser, J. David Neelin, Justin P. Stachnik, Tong Lee, (2014a), Cloud-  
496 Precipitation-Radiation-Dynamics Interaction in Global Climate Models: A Snow and Radiation  
497 Interaction Sensitivity Experiment, *J. Geophys. Res. Atmos.*, DOI: 10.1002/2013JD021038.

498 Li, J.-L. F., D. E. Waliser, G. Stephens, S. Lee, T. L'Ecuyer, S. Kato, N. Loeb, and H.-Y. Ma (2013),  
499 Characterizing and understanding radiation budget biases in CMIP3/CMIP5 GCMs, contemporary  
500 GCM, and reanalysis, *J. Geophys. Res. Atmos.*, 118, doi:10.1002/jgrd.50378.

501 Li, J.-L. F., D. E. Waliser, W.-T. Chen, B. Guan, T. Kubar, G. Stephens, H-Y Ma, D. Ming, L. Donner, C.  
502 Seman, and L. Horowitz, (2012), An observationally based evaluation of cloud ice water in CMIP3  
503 and CMIP5 GCMs and contemporary reanalyses using contemporary satellite data, *J. Geophys.*  
504 *Res.*, doi:10.1029/2012JD017640.

505 Liou, K. K., 1986, Influence of cirrus clouds on weather and climate processes: A global  
506 perspective, *Mon. Wea. Rev.*, 114, 1167-1198.

507 Liou, K. N., 2002, An Introduction of Atmospheric Radiation, 2nd Edition, Academic Press,  
508 Chapter 8.

509 Ma, H.-Y., M. Köhler, J.-L. F. Li, et al., (2012), Evaluation of an ice cloud parameterization based  
510 on a dynamical-microphysical lifetime concept using CloudSat observations and the  
511 ERAInterim reanalysis, *J. Geophys. Res.*, 117, D05210, doi:10.1029/2011JD016275.

512 Mace, G. G., Q. Zhang, M. Vaughan, R. Marchand, G. Stephens, C. Trepte, and D. Winker (2009),  
513 A description of hydrometeor layer occurrence statistics derived from the first year of

514 merged CloudSat and CALIPSO data, *J. Geophys. Res.*, 114, D00A26,  
515 doi:10.1029/2007JD009755.

516 Michibata, T., K. Suzuki, M. Sekiguchi, and T. Takemura (2019), Prognostic precipitation in the  
517 MIROC6-SPRINTARS GCM: Description and evaluation against satellite observations. *J.*  
518 *Adv. Model. Earth Syst.*, 11, 839-860. doi:10.1029/2018MS001596.

519 Ogura, T., S. Emori, M. J. Webb, Y. Tsushima, T. Yokohata, A. Abe-Ouchi, and M. Kimoto,  
520 (2008), Towards understanding cloud response in atmospheric GCMs: The use of  
521 tendency diagnostics. *J. Meteor. Soc. Japan*, 86, 69–79.

522 Rasch, P. J., and J. E. Kristjánsson (1998), A comparison of the CCM3 model climate using  
523 diagnosed and predicted condensate parameterizations, *J. Climate*, 11, 1587–1614.

524 Rotstayn, L. D., (1997), A physically based scheme for the treatment of stratiform clouds and  
525 precipitation in large-scale models. I: Description and evaluation of the microphysical  
526 processes, *Q. J. Roy. Meteorol. Soc.*, 123, 1227-1282, 1997.

527 Rotstayn, L. D., B. F. Ryan, and J. Katzfey (2000), A scheme for calculation of the liquid  
528 fraction in mixed-phase clouds in large-scale models, *Mon. Wea. Rev.*, 128, 1070–1088.

529 Sassen, K., Z. Wang, and D. Liu (2009), Cirrus clouds and deep convection in the tropics: Insights  
530 from CALIPSO and CloudSat, *J. Geophys. Res.*, 114, D00H06,  
531 doi:10.1029/2009JD011916.

532 Schumann, U., 2002, Contrail cirrus, In Cirrus, Eds. D. K. Lynch, et al., Oxford University Press,  
533 pp.231-255.

534 Song, Xiaoliang, G. J. Zhang<sup>1</sup>, J-L F. Li (2011), Evaluation of Microphysics Parameterization for  
535 Convective Clouds in the NCAR Community Atmosphere Model CAM5, *J. Clim.*, [Vol. 25,](#)  
536 [No. 24 \(15 December 2012\)](#), pp. 8568-8590 (23 pages).

537 Sundqvist, H., E. Berge, and J. E. Kristjánsson, 1989: Condensation and cloud  
538 parameterization studies with a mesoscale numerical weather prediction  
539 model. *Mon. Wea. Rev.*, **117**, 1641–1657, [https://doi.org/10.1175/1520-](https://doi.org/10.1175/1520-0493(1989)117<1641:CACPSW>2.0.CO;2)  
540 [0493\(1989\)117<1641:CACPSW>2.0.CO;2](https://doi.org/10.1175/1520-0493(1989)117<1641:CACPSW>2.0.CO;2).

541 Stein, Thorwald H. M., Julien Delanoë, Robin J. Hogan (2011), A Comparison among Four  
542 Different Retrieval Methods for Ice-Cloud Properties Using Data  
543 from CloudSat, CALIPSO, and MODIS. *J. Appl. Meteor. Climatol.*, 50, 1952–1969. doi:  
544 10.1175/2011JAMC2646.1

545 Stephens, G. L., et al. (2009), CloudSat mission: Performance and early science after the first  
546 year of operation, *J. Geophys. Res.*, 113, D00A18, doi:10.1029/2008JD009982, [printed  
547 114(D8), 2009].

548 Sassen, K., and Z. Wang, (2008) Classifying clouds around the globe with the CloudSat radar: 1-  
549 year of results, *Geophys. Res. Lett.*, 35, L04805, doi:10.1029/2007GL032591.

550 Taylor, K. E. (2001), Summarizing multiple aspects of model performance in a single diagram, *J.*  
551 *Geophys. Res.*, 106, 7183–7192.

552 Tao, W., J. Chern, Robert Atlas, David Randall, Marat Khairoutdinov, J-L F. Li, Duane E. Waliser,  
553 A. Hou, Xin Lin, Christa Peters-Lidard, William Lau, Jonathan Jiang, and J. Simpson,  
554 2009: A Multiscale Modeling System: Developments, Applications, and Critical Issues,  
555 *Bull. Amer. Meteor. Soc.*, 90(4), 515–534.

556 Tiedtke, M. (1993), Representation of clouds in large-scale models, *Mon. Wea. Rev.*, *121*, 3040–  
557 3061.

558 Volodin, E. M., N. A. Dianskii, and A. V. Gusev, (2010), Simulating Present Day Climate with  
559 the INMCM4.0 Coupled Model of the Atmospheric and Oceanic General Circulations,  
560 ISSN 0001 4338, *Izvestiya, Atmospheric and Oceanic Physics*, 2010, Vol. 46, No. 4, pp.  
561 414–431.

562 Waliser, D. E., et al. (2009), Cloud ice: A climate model challenge with signs and expectations of  
563 progress, *J. Geophys. Res.*, *114*, D00A21, doi:10.1029/2008JD010015.

564 Waliser, D. E., J.-L. F. Li, T. S. L’Ecuyer, and W.-T. Chen (2011), The impact of precipitating  
565 ice and snow on the radiation balance in global climate models, *Geophys. Res. Lett.*, *38*,  
566 L06802, doi:10.1029/ 2010GL046478.

567 Wu, L-T and J.-L.-F. Li et al, (2015), An observationally-based evaluation of WRF regional  
568 climate simulations over the Central and Eastern Pacific, *J. Geophys.*  
569 *Res.*, DOI: 10.1002/2015JD023561.

570 Xu, K.-M., and coauthors, (2002), An intercomparison of cloud-resolving models with the ARM  
571 summer 1997 IOP data. *Q. J. Roy. Meteor. Soc.*, *128*, 593-624.

572 Young, Stuart A., Mark A. Vaughan (2009), The Retrieval of Profiles of Particulate Extinction  
573 from Cloud-Aerosol Lidar Infrared Pathfinder Satellite Observations (CALIPSO) Data:  
574 Algorithm Description. *J. Atmos. Oceanic Technol.*, *26*, 1105–1119. doi:  
575 10.1175/2008JTECHA1221.1

576 Zhang, Chengzhu, Minghuai Wang, Hugh Morrison, Richard C. J. Somerville, Kai Zhang,  
577 Xiaohong Liu, J.-L. F. Li, (2014), Investigating Ice Nucleation in Cirrus Clouds with an

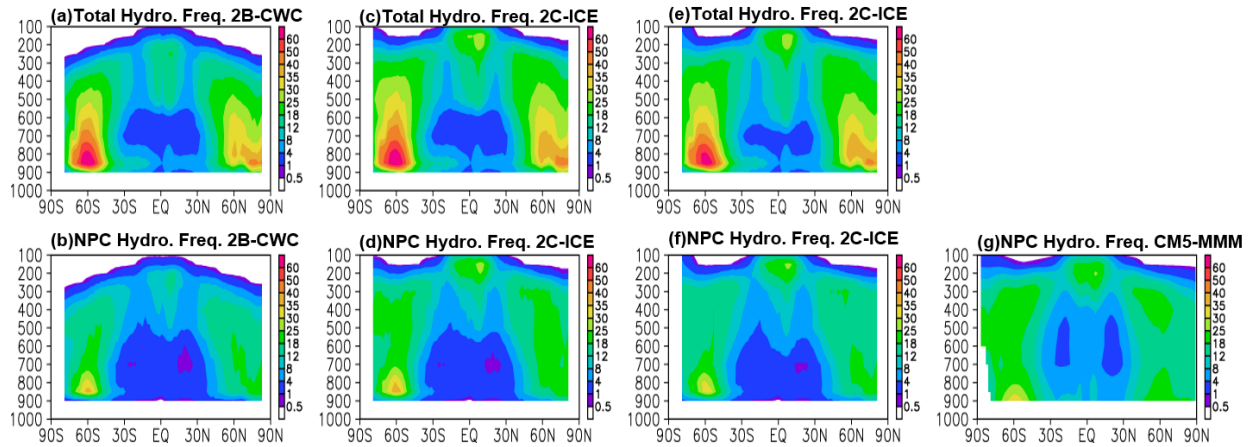
578 Aerosol-enabled Multi-scale Modeling Framework. *J. Adv. Model. Earth Syst.*, DOI:  
579 10.1002/2014MS000343.

580

581

582 **FIGURES**

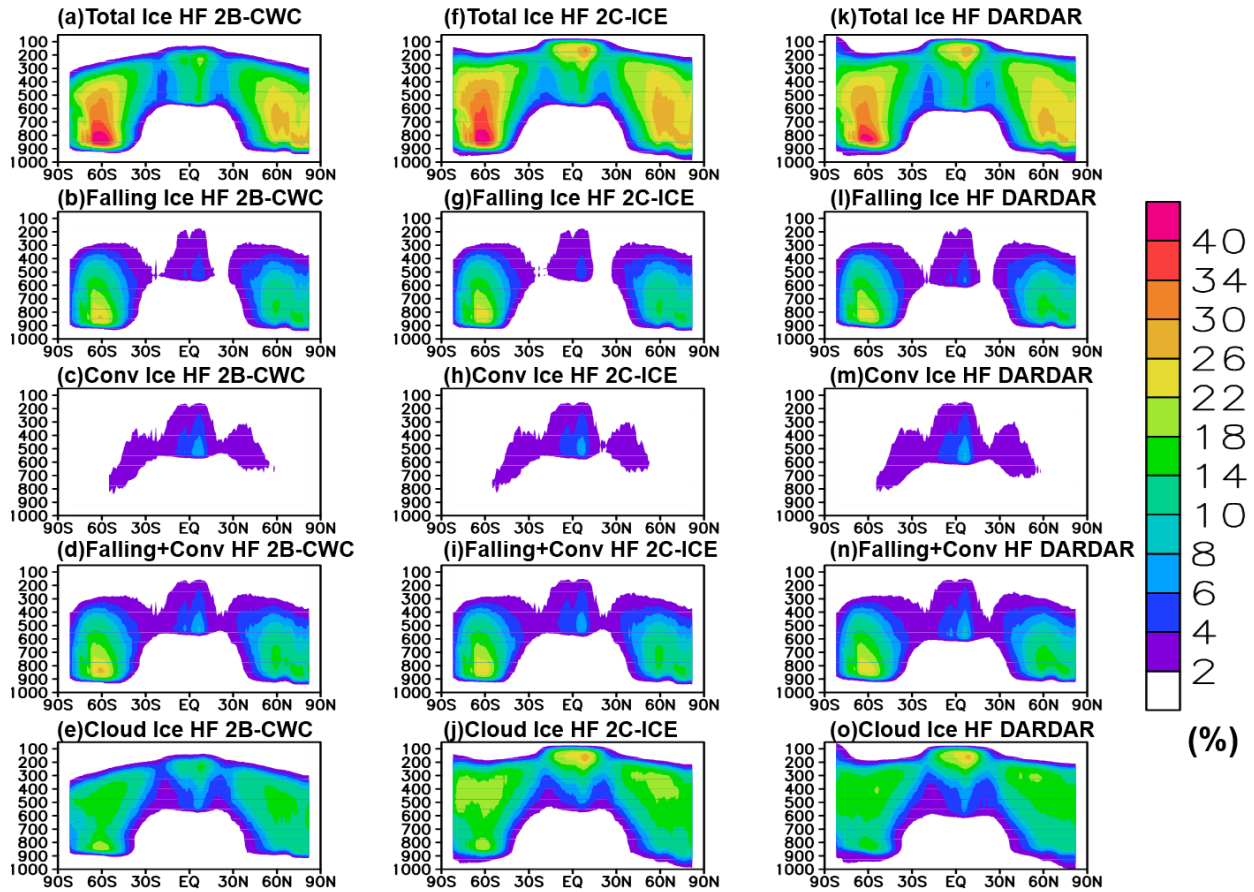
583



584

585 **Figure 1.** (a) Zonally-averaged annual means of total radiatively-active hydrometeor frequency  
586 from 2B-CWC data product, (b) same as (a) but for non-precipitating and non-convective  
587 hydrometeor frequency, which combines floating ice with floating liquid HFs. (c)—(d) same as  
588 (a)—(b) but for 2C-ICE data product. (e)—(f) same as (a)—(b) but for DARDAR data product.  
589 Floating liquid HF from 2B-CWC is used in (a-f). (g) same as (b) but for CMIP5 multi-model-  
590 mean (MMM) cloud fraction in 1980-2005. Units: %.

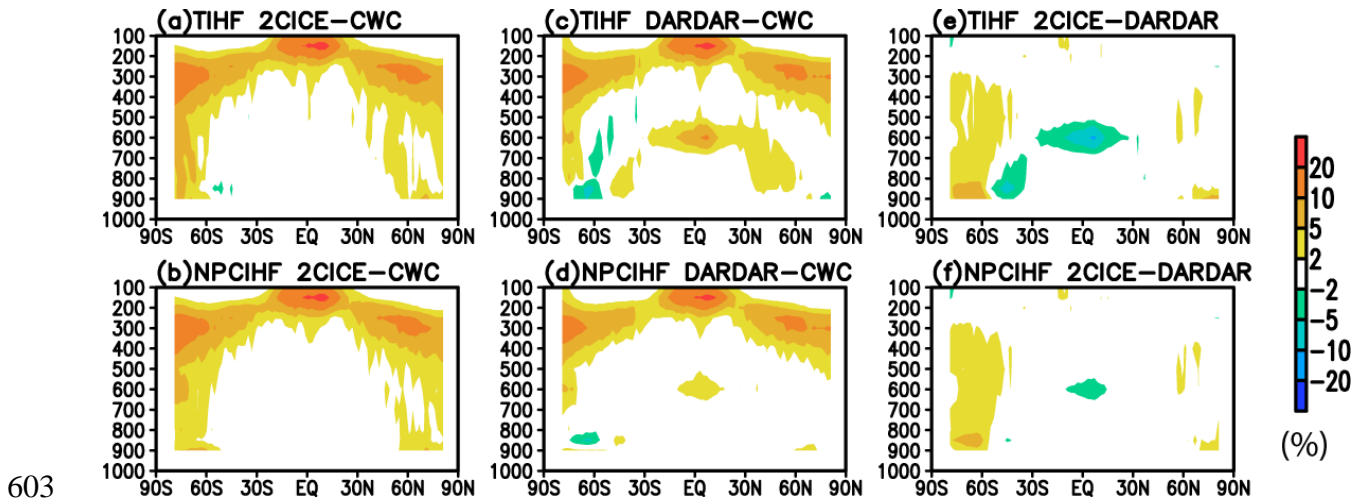
591



592

593 **Figure 2.** Zonally-averaged annual mean of (a) total ice hydrometeor frequency (TIHF), (b)  
 594 precipitating ice hydrometeor frequency (PIHF), (c) convective ice hydrometeor frequency  
 595 (CIHF), (d) sum of precipitating and convective ice hydrometeor frequency and (e) floating ice  
 596 hydrometeor frequency (FIHF) from 2B-CWC CloudSat radar only; (f)—(j) same as (a)—(e) but  
 597 for 2C-ICE derived from both the CloudSat radar and CALIPSO lidar; (k)—(n) same as (a)—(e)  
 598 but from DARDAR derived from both the CloudSat radar and CALIPSO lidar for period of 2007—  
 599 2010. The hydrometeors frequencies are estimated based on surface precipitation and/or  
 600 convective cloud flags. See Li et al. (2012) for the details and references for these methods. Unit  
 601 is %.

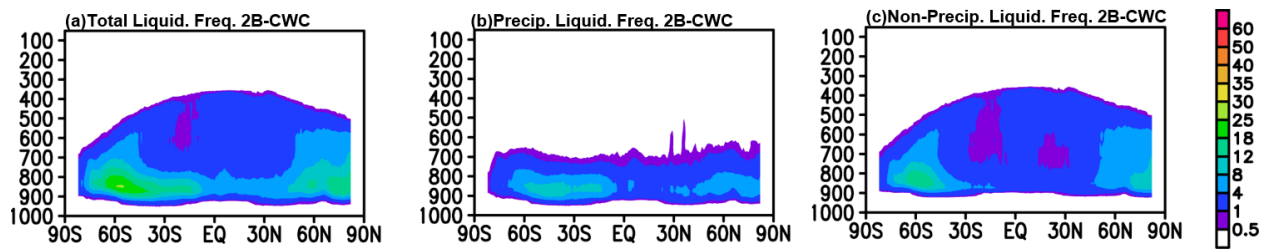
602



603  
 604 **Figure 3.** Zonally-averaged annual mean difference of (a) total ice hydrometeor frequency (TIHF)  
 605 between 2C-ICE and 2B-CWC (CWC), (b) same as (a) but for non-precipitating and non-  
 606 convective ice hydrometeor frequency (NPCIHf), (c)—(d) same as (a)—(b) but for the difference  
 607 between DARDAR and 2B-CWC (CWC), (e)—(f) same as (a)—(b) but for the difference between  
 608 2C-ICE and DARDAR for period of 2007—2010.

609

610



611

612 **Figure 4.** Zonally-averaged annual mean of (a) total liquid hydrometeor frequency (TLHF)

613 which is summed of (b) precipitating liquid hydrometeors (PLHF) and (c) non-precipitating

614 (NPCLHF). Units: %.

615

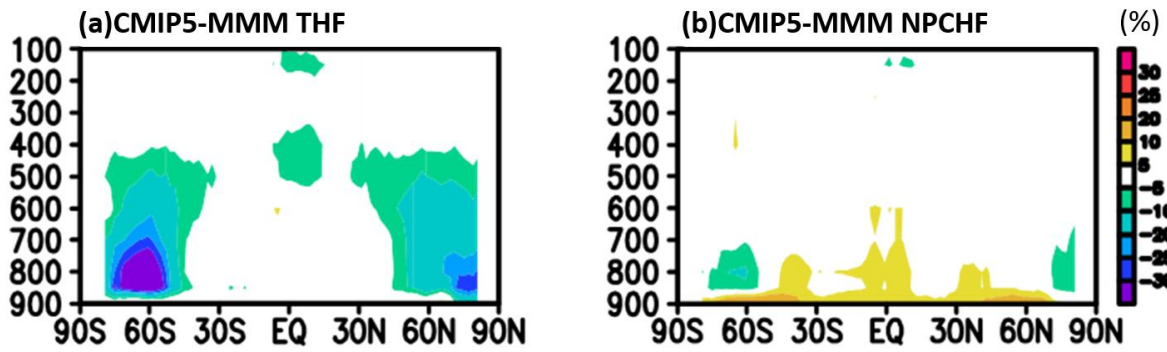
616

617

618

619

620

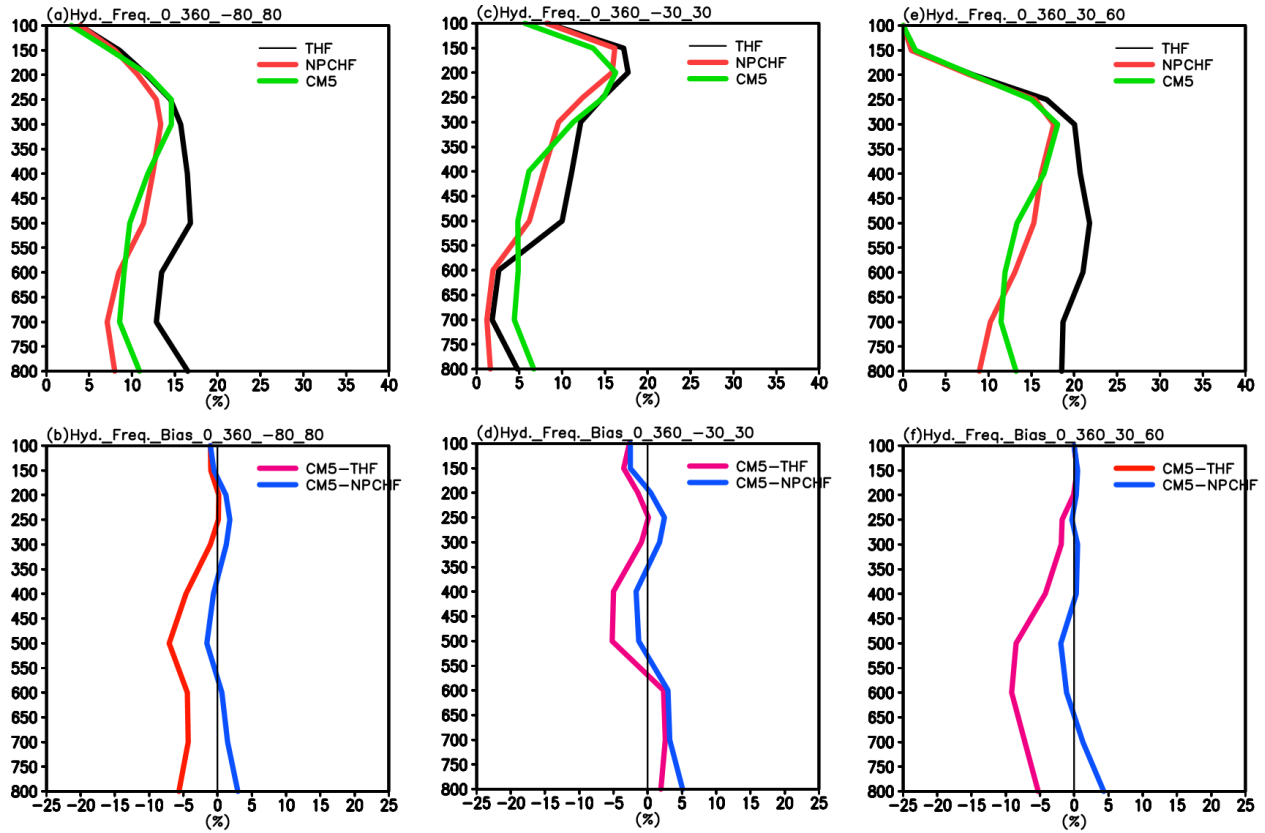


621

622 **Figure 5.** (a) CMIP5 multi-model-mean (CMIP5-MMM) zonally-averaged cloud fraction bias  
623 against total hydrometeor frequency (ice+liquid+snow) (TOT) from 2B-CWC +2C-ICE, (b) same  
624 as in (a) but against stratiform “cloud only (ice+liquid)” (NPCHF) from 2B-CWC+2C-ICE. Units:  
625 %.

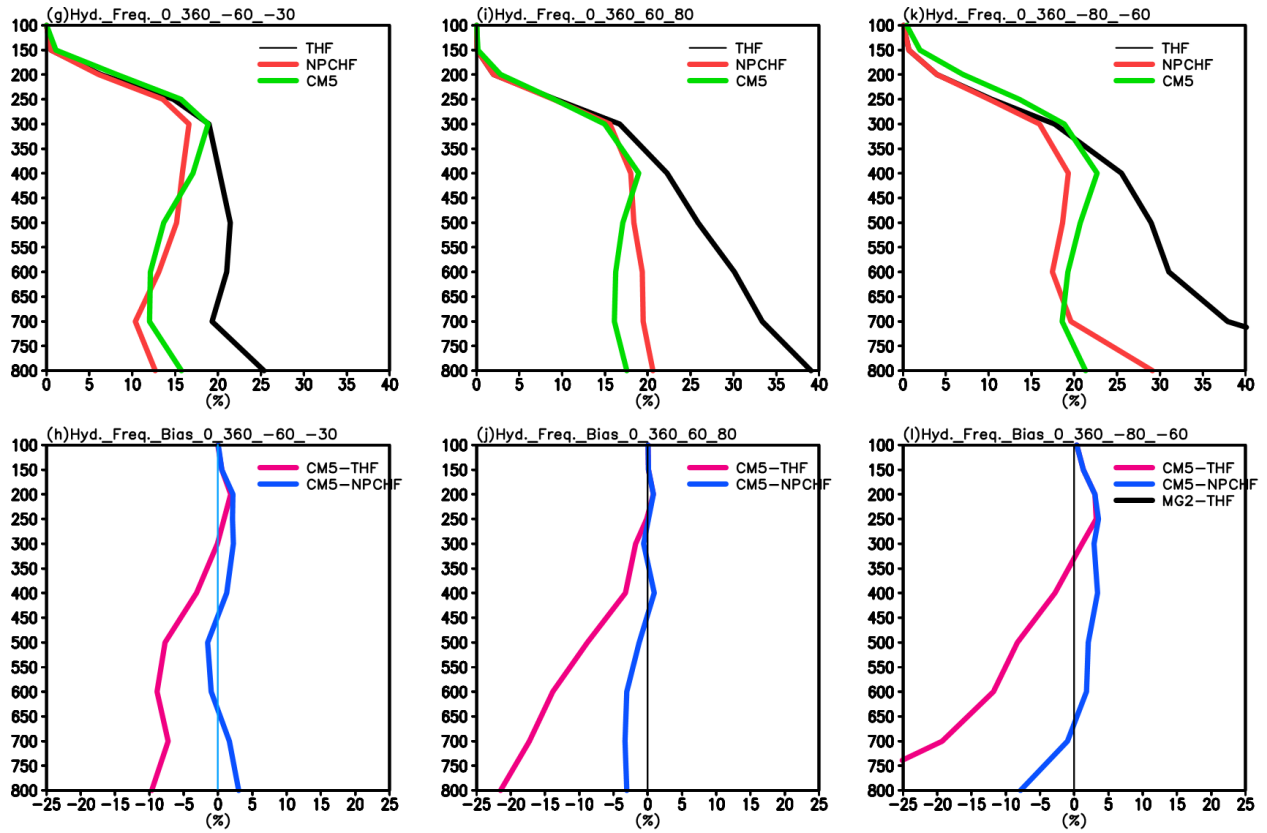
626

627



628

629 **Figure 6.** (a) Regional average hydrometeor frequency profiles of total (TOT: red color), non-  
 630 precipitation and non-convective HF (NPC: blue) and CMIP5-MMM (MMM: black) cloud  
 631 fraction average over the nearly global domain (80 S – 80N), (b) Same as (a) but for the differences  
 632 of profile of CMIP5 MMM against NPCHF (blue) and THF (red) estimates; (c)—(d) Same as  
 633 (a)—(b) but for the area average over the tropics (30 S – 30N); (e)—(f) Same as (a)—(b) but for  
 634 NH midlatitudes (30 N – 60 N), (g)—(h) Same as (a)—(b) but for SH midlatitudes (30 S – 60 S),  
 635 (i)—(j) Same as (a)—(b) but for NH high latitudes (60 N – 80 N), (k)—(l) Same as (a)—(b) but  
 636 for SH high latitudes (60 S – 80 S). Units: %.

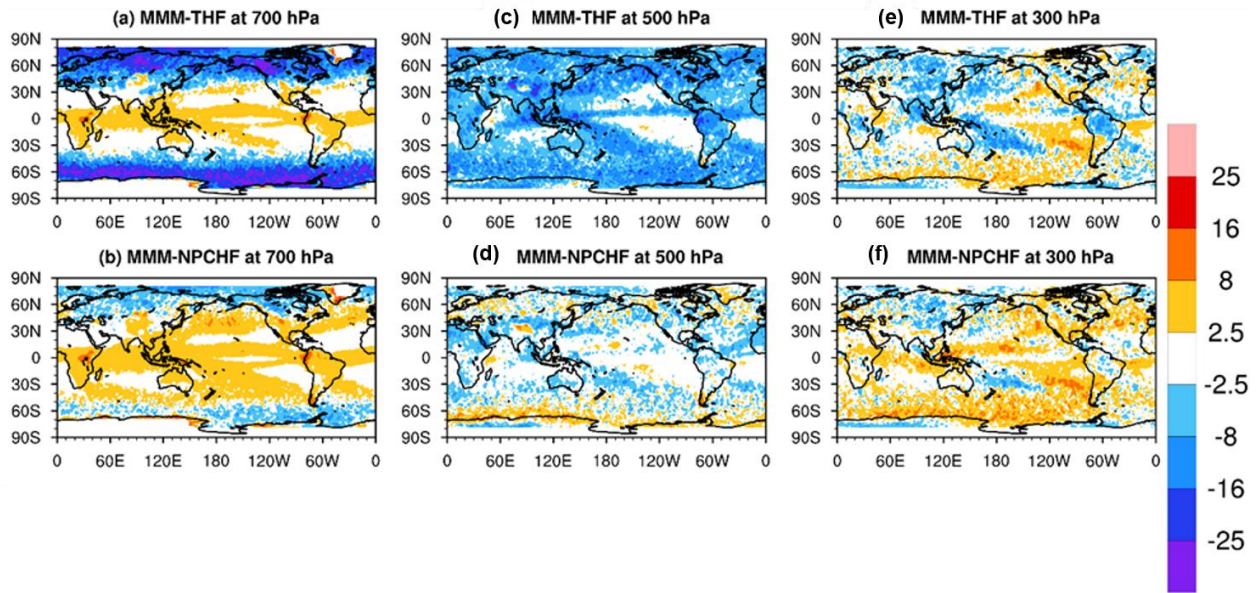


637

638 **Figure 6** continue.

639

640



641

642 **Figure 7.** (a) CMIP5 multi-model means (MMM) cloud fraction biases at 700 hPa against the  
643 estimated total hydrometeor fraction (THF), (b) same as (a) but against the estimated cloud-only  
644 hydrometeor fraction (NPCHF); (c)—(d) same as (a)—(b) but at 500 hPa; (e)—(f) same as (a)—  
645 (b) but at 300 hPa. Units: %.

646

647 **APPENDIX**

648 **TABLE**

649 **Table A1a.** Model label, number of model grids, institution and model full name of CMIP5  
 650 models examined in this study.

<b>Model Label</b>	<b>Number of model grids (x, y, and z)</b>	<b>Institution/Full Model Name</b>
GISS-E2-R	90x144x29	NASA / Goddard Institute for Space Studies, USA/GISS-E2-R
Inmcm4	120x180x21	Institute for Numerical Mathematics, Russia/Inmcm4
IPSL	96x96x39	Institute Pierre Simon Laplace, France/IPSL-CM5A-LR
MIROC	64x128x80	University of Tokyo, NIES, and JAMSTEC, Japan/MIROC-ESM-CHEM
MIROC-ESM	64x128x80	University of Tokyo, NIES, and JAMSTEC, Japan/MIROC-ESM
MRI-CGCM3	160x320x35	Meteorological Research Institute, Japan/MRI-CGCM3
NorESM	96x144x26	Norwegian Climate Centre, Norway/NorESM1-M
CSIRO	96x192x18	Australian Commonwealth Scientific and Industrial Research Organization, Australia/CSIRO-Mk3-6-0
MPI-ESM-LR	192x96x47	Max Planck Institute for Meteorology, Germany/MPI- ESM-LR

651

652 **Table A1b.** Outline of cloud microphysics and cloud fraction parameterizations used in the CMIP5  
 653 models listed in Table A1a.

Models	Prognostic cloud variables	Bulk single moment or double moment	Cloud fraction (PDF based or Non-PDF based)	References
GISS-E2-R	Single mixing ratio of total water  Diagnostic precipitating snow	Bulk single moment;  mixing ratio of cloud condensate with temperature dependent partitioning (The bounds are adjustable constants with current settings of ice $T = -35^{\circ}\text{C}$ and liquid at $T = -4^{\circ}\text{C}$ over ocean; $T = -35^{\circ}\text{C}$ and liquid at $T = -10^{\circ}\text{C}$ over land).	Diagnostic, non-PDF based	<i>Del Genio et al. (1996)</i>
Inmcm4	Mixing ratio of cloud liquid and ice	Bulk single moment  Large scale condensation in the case of relative humidity exceeds 1.	Diagnostic, non-PDF based	<i>Volodin et al., (2010)</i>
IPSL	Single mixing ratio of total water	Bulk single moment;  mixing ratio of cloud condensate with temperature dependent partitioning (The bounds are adjustable constants with current settings ice at $T = -15^{\circ}\text{C}$ and liquid at $T = 0^{\circ}\text{C}$ ).	Diagnostic PDF based	<i>Bony and Emanuel (2001)</i>
MIROC and MIROC-ESM	Mixing ratio of cloud liquid and ice	Bulk single moment;  different phases determined by temperature	Diagnostic PDF scheme with minor change for calculating  anvil cloud	<i>Ogura et al. (2008)</i> <i>Le Treut and Li, (1991);</i> <i>Hourdin et al. (2006)</i>
MRI-CGCM3	Mixing ratio of cloud liquid and ice	Double moment scheme.	Diagnostic PDF based	<i>Tiedtke (1993)</i> <i>Yukimoto et al. (2011)</i>
NorESM1	Single mixing ratio of total water	Bulk single moment;  mixing ratio of cloud condensate with temperature dependent	Diagnostic, non-PDF based	<i>Rashe and Kristjánsson (1998)</i>

		partitioning (The bounds are adjustable constants with current settings ice at T = -40oC and liquid at T = -10oC).		<i>Zhang et al. (2003)</i> <i>Boville et al. (2006)</i>
CSIRO-Mk3.6.0	Mixing ratio of cloud liquid and ice; Diagnostic precipitating snow	Bulk single moment; ice crystal number concentration is diagnosed; mixing ratio of cloud condensate with temperature dependent partitioning (The bounds are adjustable constants with current settings ice at T = -40°C );	Diagnostic, non-PDF based	<i>Rotstayn et al. (1997)</i> <i>Rotstayn et al. (2000)</i>
MPI-ESM-LR	Mixing ratio of cloud liquid and ice		cloud fraction is calculated diagnostically as a function of relative humidity	Sundqvist et al. ( <a href="#">1989</a> )

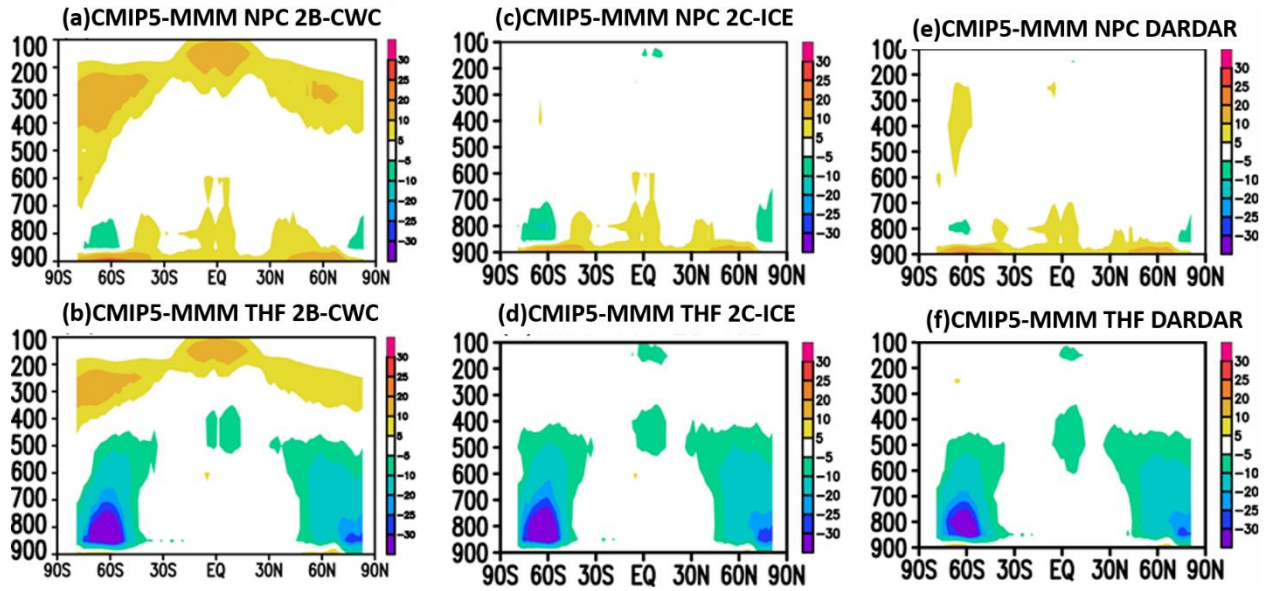
654

655

656

657

658



659

660 **Figure A1.** (a) CMIP5 multi-model-mean (MMM) zonally-averaged annual mean cloud fraction  
661 biases, compared to non-precipitating and non-convective (NPC) hydrometeor frequency (HF)  
662 estimated from 2B-CWC; (b) same as in (a) but against total radiatively-active hydrometeor  
663 frequency (ice+liquid+snow) (THF) from 2B-CWC; (c)—(d) same as in (a)—(b) but for 2C-ICE;  
664 (e)—(f) same as (a)—(b) but for DARDAR. Units: %.

665

666

1  
2 **Radiatively Active Hydrometeors Frequencies from CloudSat-CALIPSO Data for**  
3 **Evaluating Cloud Fraction in Global Climate Models**

4  
5 **Li, Jui-Lin F.<sup>1,2</sup>, \*\*Wei-Liang Lee<sup>3</sup>, Kuan-Man Xu<sup>4</sup>, Yu-Cian Tsai<sup>5</sup>, Jonathon Jiang<sup>1</sup>, Jia-**  
6 **Yuh Yu<sup>5</sup>, Graeme Stephens<sup>1</sup>, Eric Fetzer<sup>1,2</sup>, W-T Chen<sup>6</sup>**

7  
8 *<sup>1</sup>Jet Propulsion Laboratory, California Institute of Technology, Pasadena, CA, USA*

9 *<sup>2</sup>Joint Institute for Regional Earth System Science and Engineering, University of California, Los*  
10 *Angeles, CA, USA*

11 *<sup>3</sup>Research Center for Environmental Changes, Academia Sinica, Taipei, Taiwan*

12 *<sup>4</sup>Science Directorate, NASA Langley Research Center, Hampton, VA, USA*

13 *<sup>5</sup>Department of Atmospheric Sciences, National Central University, Taoyuan City, Taiwan*

14 *<sup>6</sup>Department of Atmospheric Sciences, National Taiwan University, Taipei City, Taiwan*

15  
16 **Submitted to *J. Geophys. Res. Atmos.***

17 ***Jet Propulsion Laboratory/NASA, CalTech***

18  
19 © 2022. All rights reserved.

20 2022

21  
22 **\*\*Corresponding Author: Wei-Liang Lee: [leelupin@gate.sinica.edu.tw](mailto:leelupin@gate.sinica.edu.tw)**

23 **Abstract**

24 This study derives radiatively-active hydrometeors frequencies (HFs) from CloudSat-CALIPSO  
25 satellite data to evaluate cloud fraction in present-day simulations by CMIP5 models. Most CMIP5  
26 models do not consider precipitating and/or convective hydrometeors but CESM1-CAM5 in  
27 CMIP5 has diagnostic snow and CESM2-CAM6 in CMIP6 has prognostic precipitating ice (snow)  
28 included. However, the models do not have snow fraction available for evaluation. Since the  
29 satellite-retrieved hydrometeors include the mixtures of floating, precipitating and convective ice  
30 and liquid particles, a filtering method is applied to produce estimates of cloud-only HF (or  
31 NPCHF) from the total radiatively-active HF (THF), which is the sum of NPCHF, precipitating  
32 ice HF and convective HF. The reference HF data for model evaluation include estimates of liquid-  
33 phase NPCHF from CloudSat radar-only data (2B-CWC) and ice-phase THF from CloudSat-  
34 CALIPSO 2C-ICE combined radar/lidar data. The model evaluation results show that cloud  
35 fraction from CMIP5 multi-model mean (MMM) is significantly underestimated (up to 30 %)   
36 against the total HF estimates, mainly below the mid-troposphere over the extratropics and in the  
37 upper-troposphere over the midlatitude lands and a few tropical convective regions. The CMIP5  
38 cloud fraction biases are reduced dramatically when compared to the cloud-only HF estimates, but  
39 the area of overestimates expands from the tropical convective regions to mid-latitudes in the lower  
40 and upper troposphere. There is no CMIP5 standard output snow fraction available for comparison  
41 against CloudSat-CALIPSO estimate. The implications of these results show that hydrometeors  
42 frequency estimates from CloudSat-CALIPSO provide a reference for GCM's cloud fraction from  
43 stratiform and convective form.

44

45

46 **The three key points:**

47 **Key point #1:** Deriving non-precipitating and non-convective (cloud only) and total radiatively-  
48 active hydrometeor frequency (HF) from CloudSat-CALIPSO data.

49 **Key point #2:** Cloud fractions from CMIP5 multi-model-mean compare well to cloud-only HF  
50 estimates, implying severely underestimated against total HF estimates.

51 **Key point #3:** Hydrometeors frequency estimates from CloudSat-CALIPSO provides a reference  
52 for GCM's cloud fraction from stratiform and convective form.

53

## 54 **1. Introduction**

55 Both the frequency and mass of radiatively active hydrometeors, including floating cloud  
56 ice and liquid, precipitating hydrometeors (snow), and convective ice and liquid, are important for  
57 atmospheric shortwave (SW) and longwave (LW) radiation computation (Li et al., 2013, 2018;  
58 Waliser et al., 2011; Gettelman et al., 2010; Gettelman and Morrison, 2015; Michibata et al., 2019).  
59 However, most general circulation models (GCMs), such as those participating in the 5<sup>th</sup> phase of  
60 Coupled Model Intercomparison Project (CMIP5) (Taylor et al., 2001; Gleckler et al., 2011), and  
61 the 6<sup>th</sup> phase (CMIP6) (except the CESM2-CAM6 family that considers snow-radiative effects)  
62 only consider the mass and frequency of floating cloud ice and liquid, ignoring radiatively  
63 important precipitating hydrometeor and convective core hydrometeor. Thus, the modeled  
64 atmospheric heating profiles and possibly the global radiation balance may be impacted by the  
65 missing hydrometeors because atmospheric radiation is sensitive to the broader range of  
66 hydrometeors (Li et al., 2012; Waliser et al., 2009). The miscounted or misrepresented mass of  
67 precipitating ice and convective core hydrometeors result in underestimated total ice water content  
68 and path (Li et al., 2012), which are expected to contribute to model biases of radiation budget (Li  
69 et al., 2013). Our previous studies have been focusing on characterizing and diagnosing systematic  
70 biases in the CMIP3/CMIP5/CMIP6 models associated with the precipitating ice radiative effects  
71 as well as the biases in weather models such as the European Centre for Medium-range Weather  
72 Forecast (ECMWF) (Li et al., 2014b). For example, these biases produce underestimated land  
73 surface temperature (Li et al., 2016b), overestimated sea ice concentration (Li et al., 2022) and  
74 have impacts on the modeled sea surface temperatures (Li et al., 2014a, 2016a, b, 2021).

75 While the aforementioned systematic biases contributed by ignoring the precipitating  
76 hydrometeors mass exist in many GCMs, it is essential to evaluate their performance in terms of

77 the frequency (fraction) of radiatively active hydrometeors because it also contributes to  
78 atmospheric radiation in GCMs. However, satellite observations (e.g., CloudSat and CALIPSO)  
79 only provide retrievals of the total water mass for liquid and ice, which is the sum of floating  
80 water/ice and precipitating water/ice in stratiform clouds and convective cores (Li et al., 2012).  
81 Therefore, they are not suitable for direct comparisons with the mass and frequency of non-  
82 precipitating and non-convective hydrometeors produced by most GCMs. To separate the floating  
83 cloud ice from precipitation and convective cores, Chen et al. (2011) and Li et al. (2012) developed  
84 filtering methods to provide (floating) cloud ice water content (CIWC). These concepts and  
85 datasets have been widely employed by the scientific community. For example, Gettelman et al.  
86 (2010) used CIWC to evaluate new ice cloud microphysical approaches for the Community  
87 Atmosphere Model version 5 in the Community Earth System Model version 1 (CESM1-CAM5)  
88 and to develop a new convection scheme with convective cloud ice mass included in CAM5 (Song  
89 et al., 2012). Zhang et al. (2014) investigated ice nucleation in cirrus clouds. The dataset has also  
90 been used to evaluate the IWC representation in the UCLA GCM (Ma et al., 2012), the Weather  
91 Research and Forecasting (WRF) model (Wu et al., 2015), and the Goddard Multiscale Modeling  
92 System (Tao et al., 2009). Another approach is to use satellite simulator software for model  
93 assessment (Bodas-Salcedo et al., 2011), such as using the GCM-Oriented CALIPSO Cloud  
94 Product (CALIPSO-GOCCP) (Cesana et al., 2016), and to evaluate model's cloud phase transition  
95 and low cloud feedback (Cesana et al., 2019). But this approach does not separate the different  
96 types of hydrometeors frequency and might miss the frequency of large particles, which are  
97 detected by CloudSat radar but not by CALIPSO lidar (Cesana et al., 2019).

98           It is noted that the aforementioned studies have focused on the mass and radiative effects  
99 of cloud and precipitating hydrometeors. In this study, we turn our perspective to the occurrence

100 of the radiatively active hydrometeor frequency (HF), which is generally considered equivalent to  
101 the cloud fraction except for sampling cloud fields at a fixed location in time (Clothiaux et al.,  
102 2009; Xu et al., 2012) or on a narrow satellite swath in space such as CloudSat and CALIPSO.  
103 The objective of this study is to provide an observational estimate to evaluate different types of  
104 HF (cloud fraction in model output), including cloud ice, precipitating ice, and cloud liquid, from  
105 the CMIP5 models. Three retrieval algorithms, either using CloudSat radar or CALIPSO lidar or  
106 both, provide global retrievals of ice water content (IWC), including small particles (floating cloud  
107 ice) to larger particles (snow), and liquid water content (LWC), as well as the effective radius (Re)  
108 and the extinction coefficient from the thinnest cirrus (seen only by the lidar) to the thickest ice  
109 cloud (Austin et al., 2001; Hogan et al., 2006; Delanoë and Hogan, 2008, 2010; Macc et al., 2009;  
110 Young and Vaughan, 2009; Sassen et al., 2009; Deng et al., 2010; Stein et al., 2011). In this study,  
111 we use cloud liquid HF from CloudSat-only 2B-CWC-RO5 product (Austin et al., 2009; Li et al.,  
112 2018), combined with CloudSat-CALIPSO ice water products from 2C-ICE (Deng et al., 2010,  
113 2013) and DARDAR (raDAR/liDAR) (Hogan, 2006; Delanoë and Hogan, 2008, 2010) for  
114 obtaining the total HF (THF), non-precipitating and non-convective HF (NPCHF), precipitating  
115 ice HF (PIHF), and convective HF (CHF), so that a robust and meaningful observational HF  
116 estimate can be made for model evaluations.

117 In Section 2, we describe the observational resources for the estimated hydrometeor  
118 frequency from CloudSat-CALIPSO data, the separation of different types of hydrometeor  
119 frequencies and the cloud fractions in model simulations. In Section 3, we discuss the results with  
120 a summary and conclusions drawn in Section 4.

121

## 122 **2. Reference Datasets, Separation of Hydrometeors Frequency and Model output**

### 123 **2.1 Hydrometeors Frequency Reference Datasets**

124 We generate five types of HF, based on the “FLAG” method developed in Waliser et al.  
125 (2009) and Li et al. (2012, 2018), for non-precipitating and non-convective floating cloud ice  
126 (FIHF) and cloud liquid (FLHF), convective ice (CIHF) and convective liquid (CLHF), and  
127 precipitating ice (PIHF) associated with their respective masses, using CloudSat-CALIPSO  
128 measurements including 2B-CWC, 2C-ICE, and DARDAR datasets. The sum of FIHF and FLHF  
129 is also called, interchangeably, non-precipitating and non-convective HF (NPCHF) or cloud-only  
130 HF. These three datasets cover the period of January 2007 to December 2010.

131 (a) *2B-CWC-RO5* (Austin et al., 2001, 2009) is a CloudSat-only product that provides  
132 estimates of the hydrometeor content from measured radar reflectivity to constrain the  
133 retrieved mass of both liquid and ice phases for all heights.

134 (b) *DARDAR* (raDAR/liDAR) (Hogan, 2006; Delanoë and Hogan, 2008, 2010) is a synergistic  
135 ice cloud retrieval product derived from the combination of the CloudSat radar and  
136 CALIPSO lidar using a variational method for retrieving profiles of the extinction  
137 coefficient, IWC, and equivalent radius ( $R_e$ ) of the ice cloud (Brown and Francis, 1995;  
138 Francis et al., 1998; Delanoë et al., 2011; Stein et al., 2011; Delanoë and Hogan, 2010).

139 (c) *2C-ICE* (Deng et al., 2010) provides ice cloud retrieval also derived from the combination  
140 of the CloudSat radar and CALIPSO lidar. While using the same satellite input, *2C-ICE* is  
141 different from *DARDAR* in many ways, such as the vertical resolution, treatments of  
142 multiple scattering and backscattering, and assumptions of the particle size distribution.  
143 Readers desiring a more in-depth description of the *2C-ICE* algorithm should refer to Deng  
144 et al. (2010, 2013) for details.

## 145 **2.2 Separation of Hydrometeors Frequency**

146           There are two essential aspects regarding the compatibility of the hydrometeor mass and  
147 frequency between model and observation. First, CALIPSO measurements used in the DARDAR  
148 and 2C-ICE products have more sensitivity to small and thin cirrus clouds that might make very  
149 little contribution to the total ice mass and water content of clouds but could play an important role  
150 in the radiation budget (Liou, 1986, 2002; Sassen, 2003; Schumann, 2002, 2009). Second, more  
151 importantly, all three products, to first order, represent the total tropospheric ice/liquid, including  
152 “floating” cloud ice/liquid and the precipitating ice (snow) with variable sizes and terminal  
153 velocities as the combined measurements are sensitive to a wide range of particle sizes. The  
154 particle sizes, including those of particles associated with convective clouds, are generally not  
155 included as prognostic variables in all current GCMs (e.g., Li et al., 2012; Waliser et al., 2009).  
156 Furthermore, it is generally assumed that convective core areas are small relative to a grid box in  
157 a typical GCM grid box size larger than a few hundred km<sup>2</sup>. Thus, its contribution to HF and mass  
158 is not very large. Even if it is either prognostically or diagnostically determined, the relative  
159 contribution does not change. However, as the resolution in the most current state-of-the-art GCMs  
160 become higher, with grid box size smaller than 100 km<sup>2</sup> to tens of km<sup>2</sup>, the contribution of HF and  
161 mass of the convective cores should be considered.

162           In this study, we use the “FLAG-method,” following Waliser et al. (2009) and Li et al.  
163 (2012), to distinguish HFs associated with clouds with ice/liquid mass from HFs associated with  
164 precipitation and convection. This method is summarized as follows. To achieve the separation of  
165 HFs of different types, we exclude all the retrievals in any profile that are flagged as precipitating  
166 at the surface and any retrieval within the profile whose cloud type is classified as “deep  
167 convection” or “cumulus” (from CloudSat 2B-CLDCLASS dataset; Sassen and Wang, 2008). The  
168 remaining profiles are associated with clouds with floating ice/liquid mass. Their frequencies are

169 called either floating ice HF (FIHF) or floating liquid HF (FLHF), depending on the cloud phase.  
170 The frequencies of the excluded profiles associated with precipitation are called precipitating ice  
171 HF (PIHF) while precipitating liquid (rain) is not important for radiative calculation, which will  
172 not be discussed. The frequencies of the excluded profiles associated with convection are called  
173 either convective ice HF (CIHF) or convective liquid HF (CLHF), depending upon the cloud  
174 phase. The total ice hydrometeor frequency (TIHF) is the sum of FIHF, PIHF and CIHF while the  
175 total liquid HF (TLHF) is the sum of FLHF and CLHF. This methodology was used for estimating  
176 CIWP/CIWC used for CMIP3 model-data comparisons (e.g., Li et al., 2012; Waliser et al., 2009)  
177 and for model cloud parameterizations improvements in CAM5 (Gettelman et al., 2010; Song et  
178 al., 2011), as well as other applications mentioned in the introduction.

179         The caveat of the aforementioned HF separation method that we need to keep in mind is  
180 that it is impossible to completely separate floating/cloudy forms from precipitating forms, as they  
181 coexist at some height intervals. Specific retrievals of this sort will require co-located vertical  
182 velocity information, such as from a Doppler radar capability and/or a multiple frequency radar,  
183 to better characterize particle sizes that are not available yet. Thus, it is beyond the scope of this  
184 study.

### 185 **2.3 Cloud Fraction in GCMs**

186         The protocol output of cloud fraction from all CMIP5 models only includes “cloud only”  
187 fraction, which is equivalent to non-precipitating and non-convective HF (NPCHF) from  
188 observational estimate outlined above. Some CMIP5 models do consider convective ice and/or  
189 diagnostic precipitating ice (snow) hydrometeors such as CESM1-CAM5, however, the model  
190 does not have snow fraction output available. The CMIP5 simulations used in this study are listed  
191 in Table A1, which provides an outline of cloud microphysics parameterizations used in each

192 model. The historical simulation, which used observed 20<sup>th</sup>-century greenhouse gases, ozone,  
193 aerosol, and solar forcing, is analyzed. The period used for the long-term mean is 1970-2005, and  
194 if a model provided multiple members of simulations, only one of them was chosen for this  
195 evaluation. For the purposes of comparison, both the GCM and observational datasets are re-  
196 gridded into a common horizontal grid of 2° latitude by 2° longitude. Figure 1h shows the zonally-  
197 averaged cloud fraction (ice+liquid) distribution from the CMIP5 multi-model-mean (MMM).

198 In addition to the CMIP5 model output, we also discuss the CESM2-CAM6 model output.  
199 The CAM6 implements a new prognostic cloud microphysics scheme for cloud ice, liquid,  
200 precipitating ice, and rain (Gettelman and Morrison, 2015; MG2). However, the model does not  
201 provide comparable output for snow fraction for comparisons.

## 202 **3. Results**

### 203 **3.1 Observational Estimates of Hydrometeor Frequencies**

204 To account for the observational uncertainty of HFs, we produce three different estimates  
205 of HFs from 2B-CWC, 2C-ICE, and DARDAR datasets in this study. Shown in Figure 2 are the  
206 zonally-averaged HFs determined by nonzero radar/lidar reflectivity from CloudSat/CALIPSO  
207 data with the classification of precipitation and convection based on surface precipitation and  
208 convective cloud flags, respectively. These are averaged from 2007 to 2010 in time. These HFs  
209 include total ice HF (TIHF; panels a, f and k), which is the sum of precipitating ice HF (PIHF;  
210 panels b, g and l), convective ice HF (CIHF; panels c, h and m), and floating cloud ice frequency  
211 (FIHF; panels e, j and o). Panels d, i and n show the sum of PIHF and CIHF. Figures 2a-2g are for  
212 2B-CWC, Figures 2f—2j are for 2C-ICE, and Figures 2k—2o are for DARDAR.

213 Overall, the precipitating ice HF dominates the total ice HF; i.e., PIHF is 22—26% below  
214 400 hPa, compared to 30—40% of TIHF over the mid-latitudes of both hemispheres (Figures 2b,

215 2g, 2l). The convective ice HF (CIHF) contributes about 6—8% between 350—500 hPa from the  
216 tropical convective zones (Figures 2c, 2h, 2m). Cloud-only ice HF (FIHF) (Figures 2e, 2j, 2o)  
217 represents 10—26% contribution, which is smaller than the PIHF over the mid-latitudes. But FIHF  
218 is larger in the upper troposphere over the tropics and midlatitudes. This is especially true for 2C-  
219 ICE and DARDAR datasets because thin ice clouds can be detected by CALIPSO lidar, but not by  
220 CloudSat radar (2B-CWC). Nevertheless, the differences in PIHF between 2C-ICE and DARDAR,  
221 as discussed below, are much smaller, compared to their differences with 2B-CWC.

222 To see the differences between the three datasets, the total ice HF and floating ice HF  
223 differences are calculated between 2C-ICE and 2B-CWF (Figures 3a and 3b), between DARDAR  
224 and 2B-CWC (Figures 3c and 3d) and between 2C-ICE and DARDAR (Figures 3e and 3f). It is  
225 evident that TIHF (Figure 3a and 3c) and FIHF (Figure 3b and 3d) estimates from the 2C-ICE and  
226 DARDAR datasets are much larger above 300-hPa levels over the tropics and above 500-hPa  
227 levels over the mid-latitudes than the radar-only 2B-CWC data. This is due to the fact that most  
228 small ice particles in cirrus clouds detected by CALIPSO lidar (2C-ICE and DARDAR) are  
229 invisible to CloudSat radar (2B-CWC), resulting in minimal amounts of HF in 2B-CWC over the  
230 upper troposphere. Since the TIHF and FIHF differences between 2C-ICE and DARDAR datasets  
231 (Figure 3e and 3f) are only ~2%, we will use 2C-ICE as our reference to compare the observed  
232 frozen hydrometeors frequencies (i.e., FIHF, PIHF and TIHF) with CMIP5 models in this study.  
233 As discussed later, the differences in HFs between models and observational estimates are much  
234 larger than 2%.

235 We also generate estimates of total liquid HF (TLHF), precipitating liquid HF (PLHF),  
236 and floating cloud liquid HF (FLHF) based on 2B-CWC dataset, which are shown in Figures 4a-  
237 c. They, as expected, have large values in the lower troposphere but not detected below ~900 hPa

238 due to ground clutter effects of CloudSat radar. The maximum FLHF occurs between 800—900  
239 hPa in the midlatitudes while the smallest FLHP occurs above ~800 hPa in the subtropics of both  
240 hemispheres due to large-scale subsidence. Note that the precipitating liquid (rain) is not  
241 radiatively active due to its large particle size. Therefore, only FLHF and convective liquid HF are  
242 considered as parts of the total HF in this study.

243 To get the total HF (THF), we add float liquid HF (FLHF) to total ice HF (TIHF). We also  
244 add FLHF to float ice HF (FIHF) to produce the estimate of non-precipitating and non-convective  
245 HF (NPCHF), total floating HF (TFHF) or cloud-only HF. The zonally-averaged annual mean  
246 THF and NPCHF are shown for 2B-CWC (Figure 1a, b), for 2C-ICE (Figure 1c, d), and DARDAR  
247 (Figure 1e, f), respectively. These estimated HFs can be used as references for evaluating cloud  
248 fractions in GCMs. The comparisons with GCMs are shown in the following sections.

### 249 ***3.2 Comparison of zonally-averaged hydrometeor frequency***

250 Figure 5 shows the differences of CMIP5-MMM cloud fractions from the combined THF  
251 and NPCHF estimates of frozen HFs from Cloudsat-CALIPSO 2C-ICE and floating liquid HF  
252 from 2B-CWC, which are used as the reference data. Differences for CMIP5-MMM from other  
253 reference data are shown in Figure A1. The zonally-averaged CMIP5-MMM cloud fraction is  
254 substantially smaller than the estimated THF by up to 20—60% over the southern and northern  
255 hemisphere mid- and high-latitudes, as shown in Figure 5a. On the contrary, it is reasonably well  
256 described compared to the estimated NPCHF with biases within 5% (Figure 5b). The excessive  
257 cloud fraction in the mid-troposphere of the tropics might be due to the uncertainty of the  
258 missing/undetected hydrometeors from CloudSat-CALIPSO caused by the strong attenuation of  
259 radar/lidar signals under thick convective cloud regions.

260

261

### 262 *3.3 Comparison of regionally averaged profiles of hydrometeor frequency*

263 Figure 6 shows the profiles of regional area averages of CMIP5-MMM cloud fractions  
264 against the estimated NPCHF and THFs for the globe [panels (a) and (b): 80°S—80°N], tropics  
265 [panels (c) and (d): 30°S—30°N], northern hemisphere (NH) mid-latitudes [panels (e) and (f):  
266 30°N—60°N] and high-latitudes belts [panels (i) and (j): 60°N—80°N], and southern hemisphere  
267 (SH) mid-latitudes [panels (g) and (h): 30°S—60°S] and high-latitudes belts [panel (k) and (l):  
268 60°S—80°S).

269 In general, the mean cloud fractions from CMIP5-MMM over all the above-mentioned  
270 regions agree well to the estimated cloud-only HF (NPCHF) with biases within 5%, as shown in  
271 the lower panels of Figure 6. When compared to the estimated THF, the mean CMIP5-MMM cloud  
272 fractions are underestimated below 300 hPa for all the above-mentioned regions because CMIP5  
273 models do not have precipitating ice and convective cloud hydrometeors included in cloud  
274 fractions. That is, precipitating ice and convective cores do not impact radiative calculation in  
275 these models. The maximum magnitudes of underestimated CMIP5 cloud fractions could reach up  
276 to 20—25% for mid- and high-latitudes over both hemispheres (Figures 6g, 6h, 6i, 6j, 6k, 6l),  
277 mainly due to the lack of precipitating ice cloud fractions. In reality, they are contributed by mid-  
278 and high-latitudes storms and stratiform precipitating ice over the polar regions.

279

### 280 *3.4. Comparison of horizontal distributions of hydrometeor frequency*

281 Figure 7 shows the CMIP5-MMM cloud fraction biases at 700 hPa, 500 hPa, and 300 hPa  
282 against the estimated THF (Figures 7a, 7d and 7g) and NPCHF (Figures 7b, 7e and 7h). As shown  
283 in Figure 7a, at 700 hPa, it is evident that CMIP5-MMM substantially underestimates the THF

284 north of 40°N and south of 40°S over storm tracks and the Arctic and Antarctic regions due to the  
285 lack of precipitating ice in CMIP5 models. The slightly overestimated CMIP5-MMM cloud  
286 fractions over convective zones might be due to the strong attenuation of radar signals below thick  
287 convective clouds that are not detected by the CloudSat radar. Compared to the estimated cloud-  
288 only HF, CMIP5-MMM cloud fractions are overestimated over the convective zones and storm  
289 track regions but still underestimated in the polar regions, as shown in Figure 7b. In general,  
290 CMIP5-MMM cloud fractions at 700 hPa are very close to the estimated NPCHF with magnitude  
291 differences less than 8%.

292 At 500 hPa, the CMIP5-MMM cloud fractions are generally underestimated over mid- and  
293 high-latitudes storm tracks and over convectively active regions such as the ITCZ, SPCZ, and  
294 warm pool due to the lack of stratiform precipitating ice and convective ice, compared to the  
295 estimated THF, as shown in Figure 7d. In contrast, they show very small biases against the  
296 estimated NPCHF with biases less than 2.5% (Figure 7e).

297 At 300 hPa, the CMIP5-MMM cloud fractions are slightly underestimated (-2.5 — -8%)  
298 against the estimated THF (Figure 7g). The largest underestimates occur in places where  
299 precipitating ice HF is expected to be large; for example, over the storm track in the North Pacific,  
300 midlatitude lands and convectively-active regions over the SPCZ and warm pool. Interestingly,  
301 the CMIP5-MMM cloud fractions are larger than the estimated THF over the South Pacific trade-  
302 wind regions and the Southern Ocean, indicating that the CMIP5 models simulate excessive high  
303 clouds over these regions (Figure 7g and 7h). This feature over the trade-wind regions is not shown  
304 over the zonally-averaged profiles (Figures 5a, 5b and 6) due to the cancellation associated with  
305 underestimates over the SPCZ. In our previous study (Li et al., 2021), we attributed this excessive  
306 cloud fraction in CMIP5-MMM to hydrometeor-radiation-circulation coupling biases caused by

307 the lack of precipitating ice radiative effects over the convective regions, leading to weaker surface  
308 wind stress, weaker trade-winds speed (effectively moist and warm advection into the region) and  
309 warmer SSTs, consequently producing high-level convective clouds over the trade-wind regions.  
310 It seems that the southeast Pacific trade-wind region does not have clouds at 300 hPa or not as  
311 much as those in CMIP5-MMM.

312

#### 313 **4. Summary and Conclusions**

314 The radiative properties of hydrometeors that are input to radiative calculation in GCMs  
315 include the mass and hydrometeors occurrence frequency. The purpose of this study is to make  
316 judicious comparisons and evaluations of the GCM representations of cloud fraction against the  
317 satellite observations of radiatively-active hydrometeor frequencies, which are inherently the  
318 combination of cloud-only ice/liquid and precipitating ice (snow). We employ a set of satellite  
319 observations of hydrometeors, including 2B-CWC-RO5 from the CloudSat radar for cloud liquid  
320 frequency and 2C-ICE and DARDAR from the combined CloudSat radar and CALIPSO lidar  
321 retrievals for frequency of cloud ice and precipitating ice (snow+graupel+hail). Then the FLAG  
322 method developed by Li et al. (2012) is used to categorize different types of hydrometeors  
323 frequency for floating cloud liquid/ice, precipitating ice, and convective liquid/ice.

324 We examined the annual-mean zonally averaged hydrometeor frequency estimates from  
325 the 2B-CWC, 2C-ICE, and DARDAR datasets. The HF derived from the 2B-CWC radar only data  
326 does not detect small ice particles such as suspended thin cirrus while it can be captured by the  
327 CALIPSO lidar used in the 2C-ICE and DARDAR datasets. It is noted that the differences in  
328 frozen hydrometeors and total hydrometeor frequencies are trivial between 2C-ICE and  
329 DARDAR. Therefore, we choose ice HF of 2C-ICE and liquid HF from 2B-CWC as a reference

330 for evaluating model simulation of cloud fraction. The filtered frequency of non-precipitating and  
331 non-convective hydrometeors (NPCHF, also called cloud-only HF) and total HF (THF), which is  
332 the sum of NPCHF, convective liquid/ice and precipitating ice (snow) HFs, can be utilized for a  
333 sensible “apple to apple” comparison within the limitation of measurement accuracy for models  
334 that produce either cloud-only cloud fraction (CMIP5 models) or cloud fraction with snow  
335 considered for computing the associated radiative effects in GCMs (such as in CESM2-CAM6 in  
336 CMIP6), respectively. Note that the precipitating liquid (rain) is not radiatively active in all current  
337 GCMs except in new version of GISS-E3 (Li et al., 2022). However, there is no snow fraction  
338 output available in CESM2-CAM6 for model-data comparison. In this study, we can only do the  
339 model-data evaluation for cloud-only liquid and ice frequency (fraction) in the CMIP5 models.

340 We evaluated zonally-averaged cloud (only) fraction from multi-model-mean (MMM) of  
341 CMIP5 historical simulations during 1970—2005 against the estimated THF and cloud-only HF.  
342 The performance of simulated CMIP5-MMM cloud fraction is extremely well in comparison to  
343 the estimated cloud-only HF with biases within 5%, except for some overestimates over the  
344 midlatitudes of both hemispheres, probably due to the attenuation of radar/lidar signals by thick  
345 clouds. When compared to the total HF (THF), CMIP5-MMM cloud fraction is underestimated  
346 with biases more than 30% magnitudes over the mid- to high-latitudes and the deep tropics below  
347 700 hPa due to the lack of precipitating ice in the CMIP5 models. The underestimates are  
348 drastically reduced over the high latitudes, compared to CMIP5-MMM.

349 We further examined the hydrometeor frequency of the CMIP5 in terms of regionally area-  
350 averaged profiles of CMIP5-MMM cloud fraction against the estimated cloud-only and total HF  
351 for global, tropical, and mid- and high-latitudes belts. We found that the performance of CMIP5-  
352 MMM is very good for all regions against the estimated cloud-only HF profiles, agreeing with

353 each other with biases within 5%. However, compared to the estimated total HF (THF) profiles,  
354 all regionally-averaged profiles of CMIP5-MMM HF are significantly underestimated (20—25%)  
355 because the CMIP5 models do not have precipitating ice and convective hydrometeors, in  
356 particular, over the mid- and high-latitude belts and stratiform precipitating ice over the polar  
357 latitudes.

358 To better understand the characteristics of cloud fraction biases, we examined the spatial  
359 patterns of CMIP5-MMM cloud fraction biases against the estimated cloud-only and total HFs at  
360 700 hPa, 500 hPa, and 300 hPa. Compared to the total HF, the CMIP5-MMM cloud fraction at  
361 700 hPa is underestimated by as large as 25% north of 40°N and south of 40°S, including storm  
362 tracks and the Arctic and Antarctic regions, due to the lack of precipitating ice in CMIP5-MMM.  
363 It is also underestimated everywhere at 500 hPa with smaller biases than at 700 hPa and slightly  
364 underestimated over the northern hemisphere midlatitudes and SPCZ. On the other hand, CMIP5-  
365 MMM cloud fraction is overestimated over the tropical convective zones, probably caused by  
366 attenuation of radar signals below thick convective clouds. Compared to the estimated cloud-only  
367 HF at 700 hPa, the CMIP5-MMM cloud fraction biases are reduced significantly over the polar  
368 regions and it is also reduced everywhere at 500 hPa with biases less than 2.5%, but areas with  
369 overestimates increase from the tropical convective regions to the middle latitudes at 700 hPa and  
370 to the Southern Ocean at 300 hPa. It is also noted that at 300 hPa, CMIP5-MMM has overestimated  
371 cloud fractions (2.5 — 16%) over the southern Pacific trade-wind regions, indicating that the  
372 CMIP5 models tend to simulate too many high clouds over these regions, which might be related  
373 to the bias of cloud-radiation-dynamics coupling produced by the lack of precipitating ice radiative  
374 effects in the convective regions reported in Li et al. (2021).

375           In summary, while most of the CMIP5 models do not consider radiatively active  
376 precipitating ice and/or convective hydrometeor, we provide estimates of HF for cloud-only  
377 (NPCHF) so that a robust estimated HF can be used for model evaluation within the limitations of  
378 measurement accuracy, which can vary with cloud and precipitating types that cannot be qualified  
379 in this study. The results show that the HF is significantly underestimated in CMIP5 MMM (up to  
380 30 %) against the observational total HF (THF), while the CMIP5 models simulate HF quite well  
381 against observational cloud-only HF. The implications of these results on model representations  
382 of cloud fraction should include radiatively active precipitating ice and convective hydrometeor  
383 types besides the cloud-only type to have a complete model-data comparison for cloud and  
384 precipitating ice fraction.

385

386

387 **Acknowledgments**

388 The research was carried out at the Jet Propulsion Laboratory, California Institute of Technology,  
389 under a contract with the National Aeronautics and Space Administration (80NM0018D0004).  
390 This work has been supported primarily by NASA MAP project and in part by the NASA  
391 CloudSat, obs4MIPs, and NASA Making Earth System Data Records for Use in Research  
392 Environments (MEaSUREs) programs. WLL has been supported by the Ministry of Science and  
393 Technology of Taiwan under the contract MOST 110-2111-M-001-008.

394 The availability of vertically-resolved cloud hydrometeor profiles 2C-ICE (Deng et al., 2010,  
395 2013) is derived from *CloudSat*-CALIPSO (Stephens et al., 2008; Austin et al., 2009;  
396 <http://www.cloudsat.cira.colostate.edu/>).

397

398

399

400

401

402

403

404

405

406 **REFERENCES**

- 407 Austin, R., and G. L. Stephens (2001), Retrieval of stratus cloud microphysical parameters using  
408 millimeter-wave radar and visible optical depth in preparation for Cloudsat: 1. Algorithm  
409 formulation, *J. Geophys. Res.*, 106, 28,233– 28,242.
- 410 Austin, R. T., A. J. Heymsfield, and G. L. Stephens (2009), Retrieval of ice cloud microphysical  
411 parameters using the CloudSat millimeter-wave radar and temperature, *J. Geophys.*  
412 *Res.*, 114, D00A23, doi:10.1029/2008JD010049.
- 413 Bodas-Salcedo, A., M. J. Webb, S. Bony, H. Chepfer, J.-L. Dufresne, S. A. Klein, Y. Zhang, R.  
414 Marchand, J. M. Haynes, R. Pincus, and V.O. John, (2011), COSP: Satellite simulation  
415 software for model assessment. *Bull. Amer. Meteor. Soc.*, doi: 10.1175/2011BAMS2856.1
- 416 Brown, P. R. A., and P. N. Francis (1995), Improved measurements of the ice water content in  
417 cirrus using a total-water probe, *J. Atmos. Oceanic Technol.*, 12, 410–414,  
418 doi:10.1175/1520-0426(1995)012<0410: IMOTIW>2.0.CO;2.
- 419 Cesana, G., Del Genio, A. D., Ackerman, A. S., Kelley, M., Elsaesser, G., Fridlind, A. M., et al.  
420 (2019). Evaluating models' response of tropical low clouds to SST forcings using  
421 CALIPSO observations. *Atmospheric Chemistry and Physics*, 19(5), 2813–2832.  
422 <https://doi.org/10.5194/acp-19-2813-2019>.
- 423 Cesana, G., Chepfer, H., Winker, D., Getzewich, B., Cai, X., Jourdan, O., Mioche, G., Okamoto,  
424 H., Hagihara, Y., Noel, V., and Reverdy, M.: Using in situ airborne measurements to  
425 evaluate three cloud phase products derived from CALIPSO: CALIPSO Cloud Phase  
426 Validation, *J. Geophys. Res.-Atmos.*, 121, 5788–  
427 5808, <https://doi.org/10.1002/2015JD024334>, 2016.

428 Chen, W.-T. Chen, C. P. Woods, J.-L. F. Li, D. E. Waliser, J.-D. Chern, W.-K. Tao, J. H. Jiang,  
429 and A. M. Tompkins (2011), Partitioning CloudSat Ice Water Content for Comparison with  
430 Upper-Tropospheric Ice in Global Atmospheric Models, *J. Geophys. Res.*,doi:10.1029/2010JD015179.  
431

432 Clothiaux, E. E., Moran, K. P., Martner, B. E., Ackerman, T. P., Mace, G. G., Uttal, T., Mather, J.  
433 H., Widener, K. B., Miller, M. A. and Rodriguez, D. J., (1999), The Atmospheric Radiation  
434 Measurement program cloud radars: Operational modes. *J. Atmos. Oceanic Tech.*, 16, 819–  
435 827.

436 Delanoë, J., and R. J. Hogan (2008), A variational scheme for retrieving ice cloud properties from  
437 combined radar, lidar, and infrared radiometer, *J. Geophys. Res.*, 113, D07204,  
438 doi:10.1029/2007JD009000.

439 Delanoë, J., and R. J. Hogan (2010), Combined CloudSat-CALIPSO-MODIS retrievals of the  
440 properties of ice clouds, *J. Geophys. Res.*, 115, D00H29, doi:10.1029/2009JD012346.

441 Del Genio, A. D., M.-S. Yao, W. Kovari, and K. K.-W. Lo (1996), A prognostic cloud water  
442 parameterization for global climate models, *J. Climate*, 9(2), 270–304, doi:10.1175/1520-  
443 0442(1996)009<0270:APCWPF>2.0.CO;2.

444 Deng, M., G. G. Mace, Z. Wang, and H. Okamoto (2010), Tropical Composition, Cloud and  
445 Climate Coupling Experiment validation for cirrus cloud profiling retrieval using CloudSat  
446 radar and CALIPSO lidar, *J. Geophys. Res.*, 115, D00J15, doi:10.1029/2009JD013104.

447 Deng, M., G. G. Mace, Z. Wang, and R. P. Lawson (2013), Evaluation of several A-Train ice cloud  
448 retrieval products with in situ measurements collected during the SPARTICUS  
449 campaign, *J. Appl. Meteor. Climatol.*, 52, 1014–1030. doi: [10.1175/JAMC-D-12-054.1](https://doi.org/10.1175/JAMC-D-12-054.1).

450 Francis, P. N., P. Hignett, and A. Macke (1998), The retrieval of cirrus cloud properties from  
451 aircraft multi-spectral reflectance measurements during EUCREX'93, *Q. J. R. Meteorol.*  
452 *Soc.*, 124, 1273– 1291.

453 Gettelman, A., X. Liu, S. J. Ghan, H. Morrison, S. Park, A. J. Conley, S. A. Klein, J. Boyle, D. L.  
454 Mitchell, J.-L. F. Li, (2010), Global simulations of ice nucleation and ice supersaturation  
455 with an improved cloud scheme in the Community Atmosphere Model. *J. Geophys. Res.*,  
456 115, D18216, doi:10.1029/2009JD013797.

457 Gettelman, A., and H. Morrison (2015), Advanced two-moment bulk microphysics for global  
458 models. Part I: Off-line tests and comparison with other schemes. *J. Climate*, 28(3), 1268–  
459 1287, doi:10.1175/JCLI-D-14-00102.1.

460 Gleckler, P. R. Ferraro, D. E. Waliser (2011), Better use of satellite data in evaluating climate  
461 models contributing to CMIP and assessed by IPCC, Meeting Summary, EOS, Vol. 92,  
462 No. 20, 17 May 2011.

463 Hogan, R. J. (2006), Fast approximate calculation of multiply scattered lidar returns, *Appl. Opt.*,  
464 45, 5984–5992.

465 Hourdin F., I. and coauthors, (2006), The LMDZ4 general circulation model : climate performance  
466 and sensitivity to parametrized physics with emphasis on tropical convection. *Climate*  
467 *Dynamics*, 19(15) :3445-3482, DOI : 10.1007/s00382-006-0158-0.

468 Le Treut, H., and Z. X. Li, (1991), Sensitivity of an atmospheric general circulation model to  
469 prescribed SST changes: Feedback effects associated with the simulation of cloud optical  
470 properties. *Climate Dyn.*, 5, 175–187.

471 Li, J.-L. F., Gregory V Cesana, Kuan-Man Xu, Mark Richardson, Hanii Takahashi, J. Jiang,  
472 (2022), Comparisons of Simulated Radiation, Surface Wind Stress and SST Fields over  
473 Tropical Pacific by the GISS CMIP6 Versions of Global Climate Models with  
474 Observations, *Environ. Res. Commun.*, IOP, accepted.

475 Li, J.-L. F., and co-authors, (2022), Observational Evaluation of Global Climate Model  
476 Simulations of Arctic Sea Ice Pertaining to the Radiative Effects of Frozen Hydrometeors,  
477 *Environ. Res. Commun.* Volume 4, Number 2, 4 025008.

478 Li, J.-L. F., K.-M. Xu, Wei-Liang Lee, J. H. Jiang, Eric Fetzer, Graeme Stephens, Jia-Yuh Yu, and  
479 Yi-Hui Wang, 2021: Changes of south-central Pacific large-scale environment associated  
480 with hydrometeors-radiation-circulation interactions in a coupled GCM. *J. Geophys. Res.*,  
481 *125*, DOI:10.1029/2021JD034973.

482 Li, J.-L.F., Seungwon Lee, Hsi-Yen Ma, G. Stephens, and Bin Guan, (2018), Assessment of the  
483 Cloud Liquid Water from Climate Models and Reanalyses using Satellite Observations,  
484 *Terrestrial Atmospheric and Oceanic Sciences*, DOI: 10.3319/TAO.2018.07.04.01.

485 Li, J.-L. F., W.-L. Lee, J.-Y. Yu, G. Hulley, E. Fetzer, Y.-C. Chen, and Y.-H. Wang (2016b), The  
486 impacts of precipitating hydrometeors radiative effects on land surface temperature in  
487 contemporary GCMs using satellite observations, *J. Geophys. Res. Atmos.*, *120*,  
488 doi:10.1002/2015JD023776.

489 Li, J.-L. F., W.-L. Lee, Tong Lee, Eric Fetzer, Jia-Yuh Yu, (2016a), The Impacts of Cloud Snow Radiative  
490 Effects on Pacific Oceans Surface Heat Fluxes, Surface Wind Stress, and Ocean Temperatures in  
491 Coupled GCM Simulations, *J. Geophys. Res. Atmos.*, *120*, DOI: 10.1002/2014JD022538.

492 Li, J.-L. F., R. M. Forbes, D. E. Waliser, G. Stephens, S. W. Lee, (2014b), Characterizing the impacts of  
493 precipitating snow hydrometeors in the radiation using the ECMWF IFS global model, *J. Geophys.*  
494 *Res. Atmos.*, 119, doi:10.1002/2014JD021450.

495 Li, J.-L. F., W.-L. Lee, D. E. Waliser, J. David Neelin, Justin P. Stachnik, Tong Lee, (2014a), Cloud-  
496 Precipitation-Radiation-Dynamics Interaction in Global Climate Models: A Snow and Radiation  
497 Interaction Sensitivity Experiment, *J. Geophys. Res. Atmos.*, DOI: 10.1002/2013JD021038.

498 Li, J.-L. F., D. E. Waliser, G. Stephens, S. Lee, T. L'Ecuyer, S. Kato, N. Loeb, and H.-Y. Ma (2013),  
499 Characterizing and understanding radiation budget biases in CMIP3/CMIP5 GCMs, contemporary  
500 GCM, and reanalysis, *J. Geophys. Res. Atmos.*, 118, doi:10.1002/jgrd.50378.

501 Li, J.-L. F., D. E. Waliser, W.-T. Chen, B. Guan, T. Kubar, G. Stephens, H-Y Ma, D. Ming, L. Donner, C.  
502 Seman, and L. Horowitz, (2012), An observationally based evaluation of cloud ice water in CMIP3  
503 and CMIP5 GCMs and contemporary reanalyses using contemporary satellite data, *J. Geophys.*  
504 *Res.*, doi:10.1029/2012JD017640.

505 Liou, K. K., 1986, Influence of cirrus clouds on weather and climate processes: A global  
506 perspective, *Mon. Wea. Rev.*, 114, 1167-1198.

507 Liou, K. N., 2002, An Introduction of Atmospheric Radiation, 2nd Edition, Academic Press,  
508 Chapter 8.

509 Ma, H.-Y., M. Köhler, J.-L. F. Li, et al., (2012), Evaluation of an ice cloud parameterization based  
510 on a dynamical-microphysical lifetime concept using CloudSat observations and the  
511 ERAInterim reanalysis, *J. Geophys. Res.*, 117, D05210, doi:10.1029/2011JD016275.

512 Mace, G. G., Q. Zhang, M. Vaughan, R. Marchand, G. Stephens, C. Trepte, and D. Winker (2009),  
513 A description of hydrometeor layer occurrence statistics derived from the first year of

514 merged CloudSat and CALIPSO data, *J. Geophys. Res.*, 114, D00A26,  
515 doi:10.1029/2007JD009755.

516 Michibata, T., K. Suzuki, M. Sekiguchi, and T. Takemura (2019), Prognostic precipitation in the  
517 MIROC6-SPRINTARS GCM: Description and evaluation against satellite observations. *J.*  
518 *Adv. Model. Earth Syst.*, 11, 839-860. doi:10.1029/2018MS001596.

519 Ogura, T., S. Emori, M. J. Webb, Y. Tsushima, T. Yokohata, A. Abe-Ouchi, and M. Kimoto,  
520 (2008), Towards understanding cloud response in atmospheric GCMs: The use of  
521 tendency diagnostics. *J. Meteor. Soc. Japan*, 86, 69–79.

522 Rasch, P. J., and J. E. Kristjánsson (1998), A comparison of the CCM3 model climate using  
523 diagnosed and predicted condensate parameterizations, *J. Climate*, 11, 1587–1614.

524 Rotstayn, L. D., (1997), A physically based scheme for the treatment of stratiform clouds and  
525 precipitation in large-scale models. I: Description and evaluation of the microphysical  
526 processes, *Q. J. Roy. Meteorol. Soc.*, 123, 1227-1282, 1997.

527 Rotstayn, L. D., B. F. Ryan, and J. Katzfey (2000), A scheme for calculation of the liquid  
528 fraction in mixed-phase clouds in large-scale models, *Mon. Wea. Rev.*, 128, 1070–1088.

529 Sassen, K., Z. Wang, and D. Liu (2009), Cirrus clouds and deep convection in the tropics: Insights  
530 from CALIPSO and CloudSat, *J. Geophys. Res.*, 114, D00H06,  
531 doi:10.1029/2009JD011916.

532 Schumann, U., 2002, Contrail cirrus, In Cirrus, Eds. D. K. Lynch, et al., Oxford University Press,  
533 pp.231-255.

534 Song, Xiaoliang, G. J. Zhang<sup>1</sup>, J-L F. Li (2011), Evaluation of Microphysics Parameterization for  
535 Convective Clouds in the NCAR Community Atmosphere Model CAM5, *J. Clim.*, [Vol. 25,](#)  
536 [No. 24 \(15 December 2012\)](#), pp. 8568-8590 (23 pages).

537 Sundqvist, H., E. Berge, and J. E. Kristjánsson, 1989: Condensation and cloud  
538 parameterization studies with a mesoscale numerical weather prediction  
539 model. *Mon. Wea. Rev.*, **117**, 1641–1657, [https://doi.org/10.1175/1520-](https://doi.org/10.1175/1520-0493(1989)117<1641:CACPSW>2.0.CO;2)  
540 [0493\(1989\)117<1641:CACPSW>2.0.CO;2](https://doi.org/10.1175/1520-0493(1989)117<1641:CACPSW>2.0.CO;2).

541 Stein, Thorwald H. M., Julien Delanoë, Robin J. Hogan (2011), A Comparison among Four  
542 Different Retrieval Methods for Ice-Cloud Properties Using Data  
543 from CloudSat, CALIPSO, and MODIS. *J. Appl. Meteor. Climatol.*, 50, 1952–1969. doi:  
544 10.1175/2011JAMC2646.1

545 Stephens, G. L., et al. (2009), CloudSat mission: Performance and early science after the first  
546 year of operation, *J. Geophys. Res.*, 113, D00A18, doi:10.1029/2008JD009982, [printed  
547 114(D8), 2009].

548 Sassen, K., and Z. Wang, (2008) Classifying clouds around the globe with the CloudSat radar: 1-  
549 year of results, *Geophys. Res. Lett.*, 35, L04805, doi:10.1029/2007GL032591.

550 Taylor, K. E. (2001), Summarizing multiple aspects of model performance in a single diagram, *J.*  
551 *Geophys. Res.*, 106, 7183–7192.

552 Tao, W., J. Chern, Robert Atlas, David Randall, Marat Khairoutdinov, J-L F. Li, Duane E. Waliser,  
553 A. Hou, Xin Lin, Christa Peters-Lidard, William Lau, Jonathan Jiang, and J. Simpson,  
554 2009: A Multiscale Modeling System: Developments, Applications, and Critical Issues,  
555 *Bull. Amer. Meteor. Soc.*, 90(4), 515–534.

556 Tiedtke, M. (1993), Representation of clouds in large-scale models, *Mon. Wea. Rev.*, *121*, 3040–  
557 3061.

558 Volodin, E. M., N. A. Dianskii, and A. V. Gusev, (2010), Simulating Present Day Climate with  
559 the INMCM4.0 Coupled Model of the Atmospheric and Oceanic General Circulations,  
560 ISSN 0001 4338, *Izvestiya, Atmospheric and Oceanic Physics*, 2010, Vol. 46, No. 4, pp.  
561 414–431.

562 Waliser, D. E., et al. (2009), Cloud ice: A climate model challenge with signs and expectations of  
563 progress, *J. Geophys. Res.*, *114*, D00A21, doi:10.1029/2008JD010015.

564 Waliser, D. E., J.-L. F. Li, T. S. L’Ecuyer, and W.-T. Chen (2011), The impact of precipitating  
565 ice and snow on the radiation balance in global climate models, *Geophys. Res. Lett.*, *38*,  
566 L06802, doi:10.1029/ 2010GL046478.

567 Wu, L-T and J.-L.-F. Li et al, (2015), An observationally-based evaluation of WRF regional  
568 climate simulations over the Central and Eastern Pacific, *J. Geophys.*  
569 *Res.*, DOI: 10.1002/2015JD023561.

570 Xu, K.-M., and coauthors, (2002), An intercomparison of cloud-resolving models with the ARM  
571 summer 1997 IOP data. *Q. J. Roy. Meteor. Soc.*, *128*, 593-624.

572 Young, Stuart A., Mark A. Vaughan (2009), The Retrieval of Profiles of Particulate Extinction  
573 from Cloud-Aerosol Lidar Infrared Pathfinder Satellite Observations (CALIPSO) Data:  
574 Algorithm Description. *J. Atmos. Oceanic Technol.*, *26*, 1105–1119. doi:  
575 10.1175/2008JTECHA1221.1

576 Zhang, Chengzhu, Minghuai Wang, Hugh Morrison, Richard C. J. Somerville, Kai Zhang,  
577 Xiaohong Liu, J.-L. F. Li, (2014), Investigating Ice Nucleation in Cirrus Clouds with an

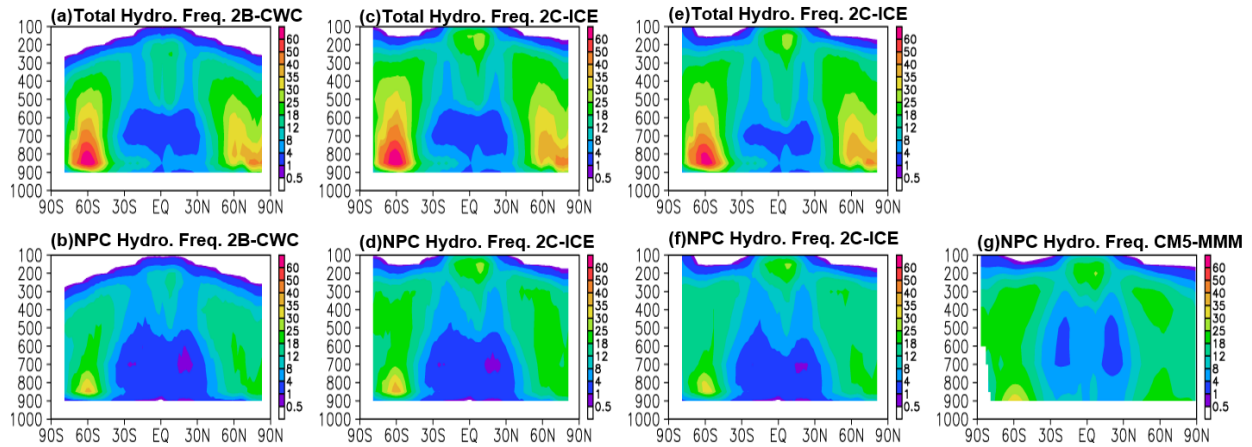
578 Aerosol-enabled Multi-scale Modeling Framework. *J. Adv. Model. Earth Syst.*, DOI:  
579 10.1002/2014MS000343.

580

581

582 **FIGURES**

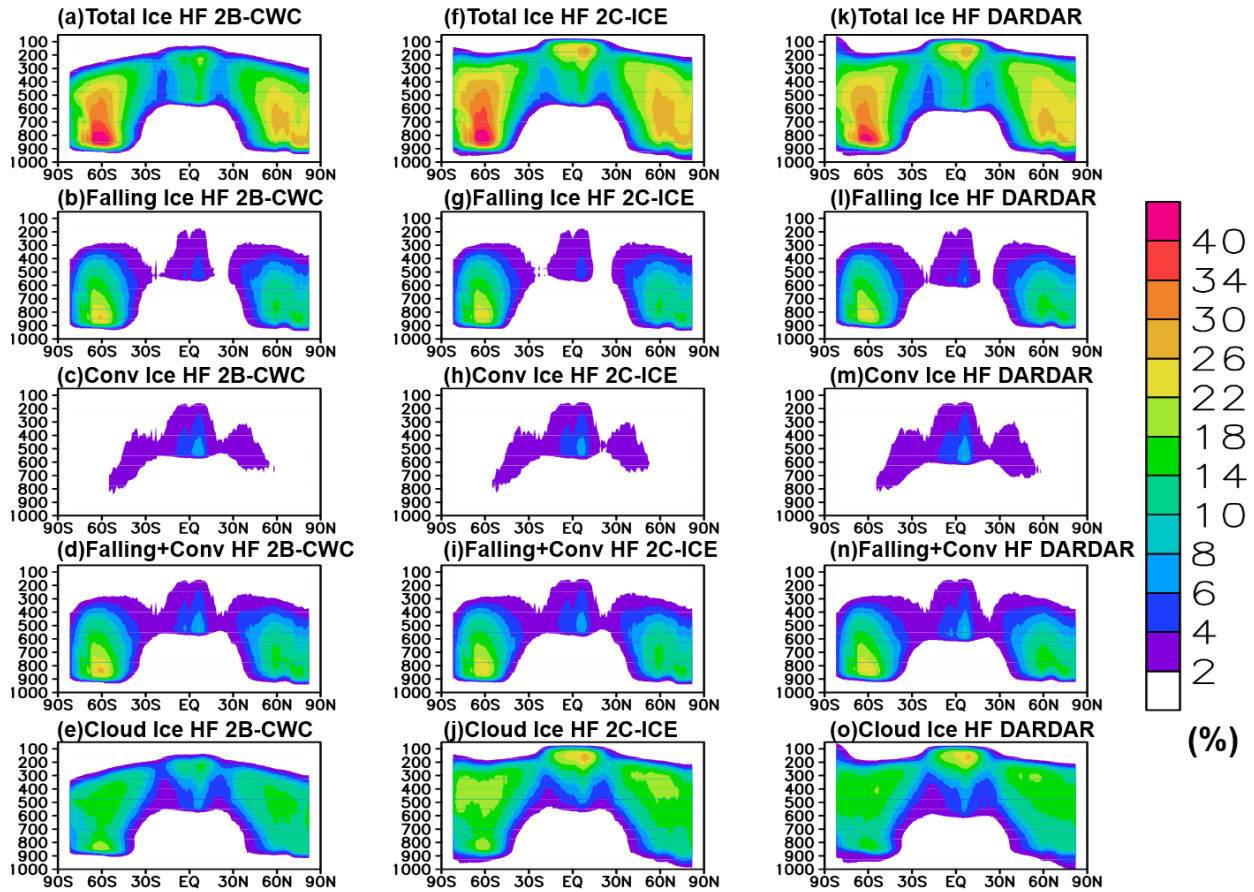
583



584

585 **Figure 1.** (a) Zonally-averaged annual means of total radiatively-active hydrometeor frequency  
586 from 2B-CWC data product, (b) same as (a) but for non-precipitating and non-convective  
587 hydrometeor frequency, which combines floating ice with floating liquid HFs. (c)—(d) same as  
588 (a)—(b) but for 2C-ICE data product. (e)—(f) same as (a)—(b) but for DARDAR data product.  
589 Floating liquid HF from 2B-CWC is used in (a-f). (g) same as (b) but for CMIP5 multi-model-  
590 mean (MMM) cloud fraction in 1980-2005. Units: %.

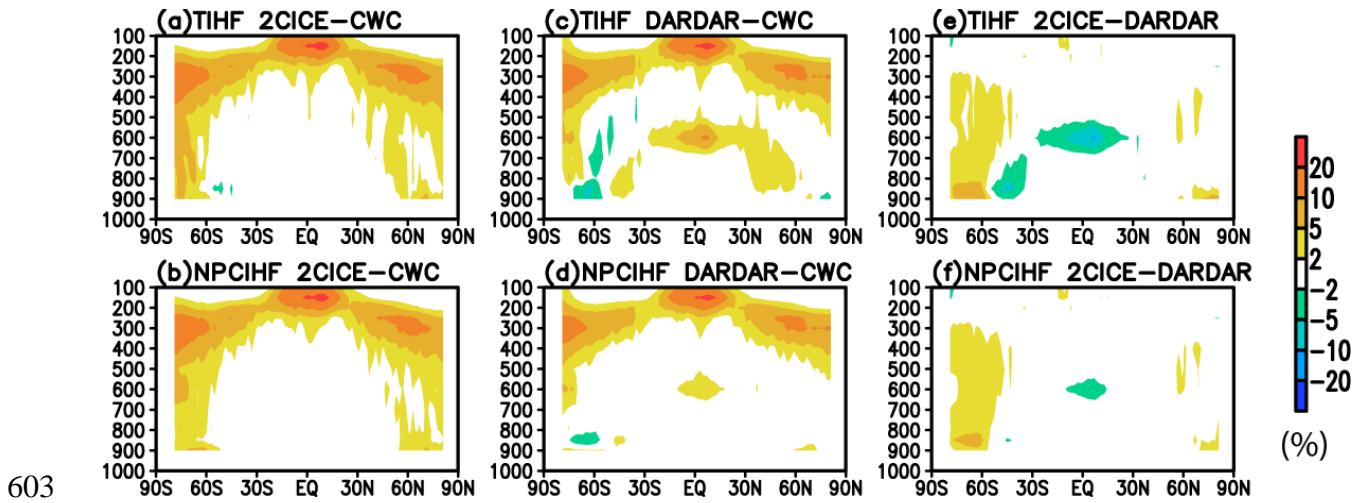
591



592

593 **Figure 2.** Zonally-averaged annual mean of (a) total ice hydrometeor frequency (TIHF), (b)  
 594 precipitating ice hydrometeor frequency (PIHF), (c) convective ice hydrometeor frequency  
 595 (CIHF), (d) sum of precipitating and convective ice hydrometeor frequency and (e) floating ice  
 596 hydrometeor frequency (FIHF) from 2B-CWC CloudSat radar only; (f)—(j) same as (a)—(e) but  
 597 for 2C-ICE derived from both the CloudSat radar and CALIPSO lidar; (k)—(n) same as (a)—(e)  
 598 but from DARDAR derived from both the CloudSat radar and CALIPSO lidar for period of 2007—  
 599 2010. The hydrometeors frequencies are estimated based on surface precipitation and/or  
 600 convective cloud flags. See Li et al. (2012) for the details and references for these methods. Unit  
 601 is %.

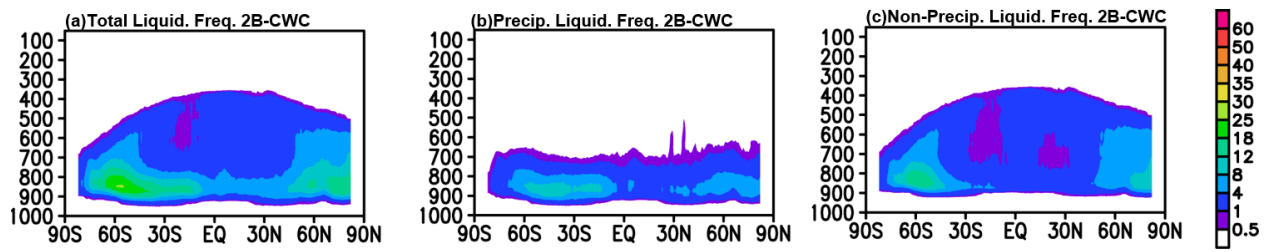
602



603  
 604 **Figure 3.** Zonally-averaged annual mean difference of (a) total ice hydrometeor frequency (TIHF)  
 605 between 2C-ICE and 2B-CWC (CWC), (b) same as (a) but for non-precipitating and non-  
 606 convective ice hydrometeor frequency (NPCIHf), (c)—(d) same as (a)—(b) but for the difference  
 607 between DARDAR and 2B-CWC (CWC), (e)—(f) same as (a)—(b) but for the difference between  
 608 2C-ICE and DARDAR for period of 2007—2010.

609

610



611

612 **Figure 4.** Zonally-averaged annual mean of (a) total liquid hydrometeor frequency (TLHF)

613 which is summed of (b) precipitating liquid hydrometeors (PLHF) and (c) non-precipitating

614 (NPCLHF). Units: %.

615

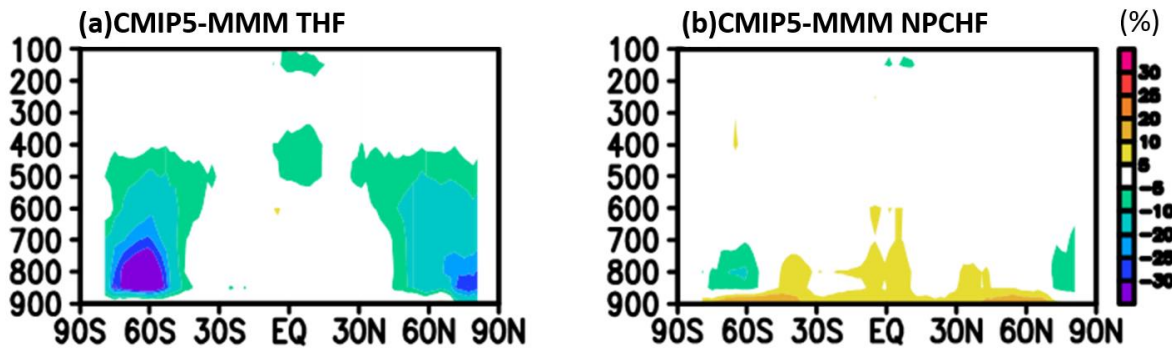
616

617

618

619

620

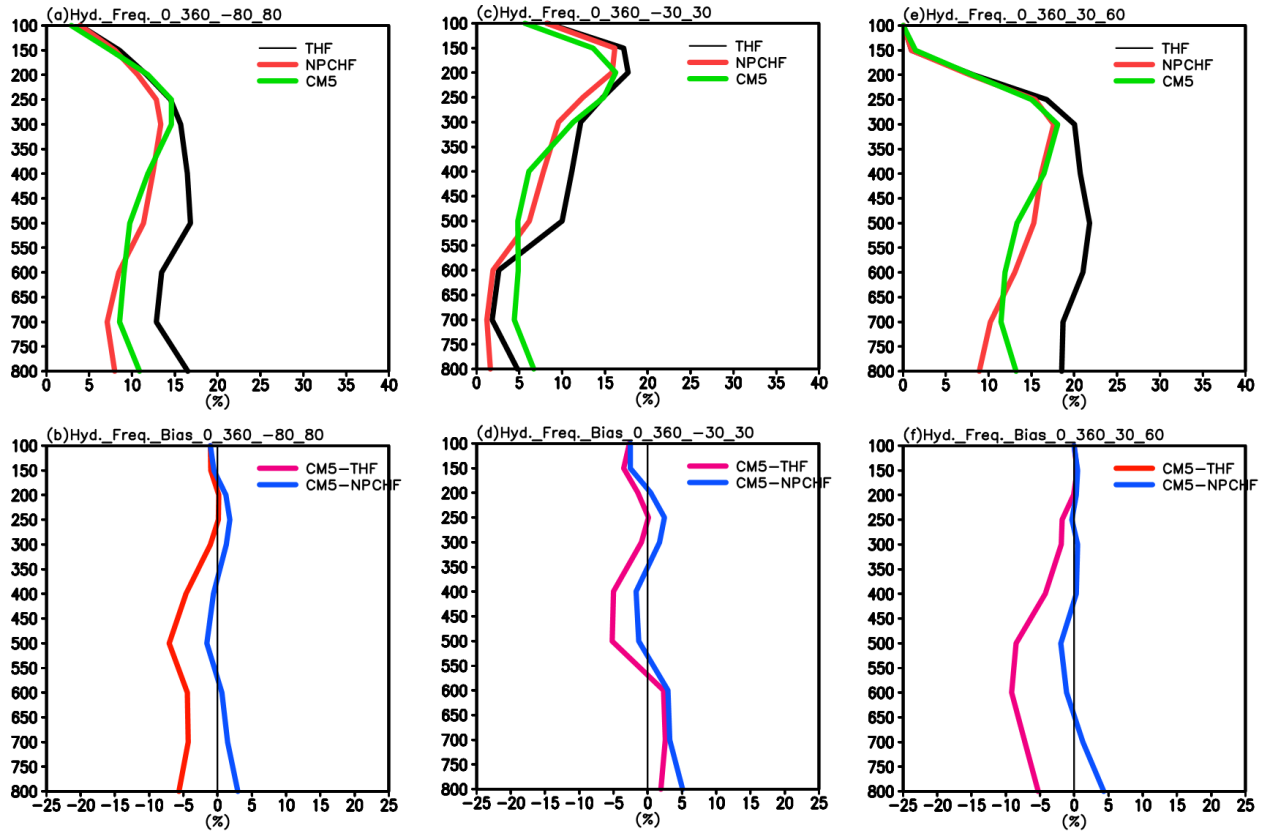


621

622 **Figure 5.** (a) CMIP5 multi-model-mean (CMIP5-MMM) zonally-averaged cloud fraction bias  
623 against total hydrometeor frequency (ice+liquid+snow) (TOT) from 2B-CWC +2C-ICE, (b) same  
624 as in (a) but against stratiform “cloud only (ice+liquid)” (NPCHF) from 2B-CWC+2C-ICE. Units:  
625 %.

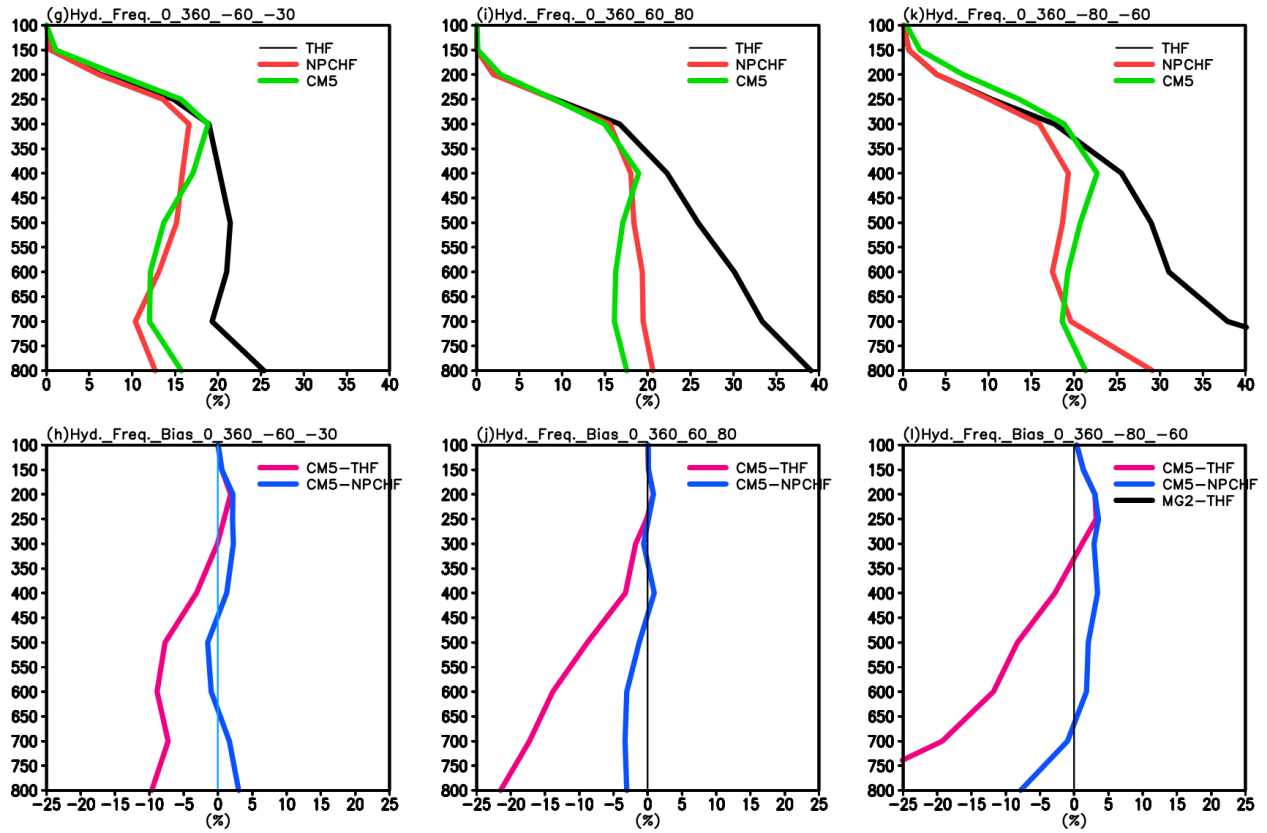
626

627



628

629 **Figure 6.** (a) Regional average hydrometeor frequency profiles of total (TOT: red color), non-  
 630 precipitation and non-convective HF (NPC: blue) and CMIP5-MMM (MMM: black) cloud  
 631 fraction average over the nearly global domain (80 S – 80N), (b) Same as (a) but for the differences  
 632 of profile of CMIP5 MMM against NPCHF (blue) and THF (red) estimates; (c)—(d) Same as  
 633 (a)—(b) but for the area average over the tropics (30 S – 30N); (e)—(f) Same as (a)—(b) but for  
 634 NH midlatitudes (30 N – 60 N), (g)—(h) Same as (a)—(b) but for SH midlatitudes (30 S – 60 S),  
 635 (i)—(j) Same as (a)—(b) but for NH high latitudes (60 N – 80 N), (k)—(l) Same as (a)—(b) but  
 636 for SH high latitudes (60 S – 80 S). Units: %.

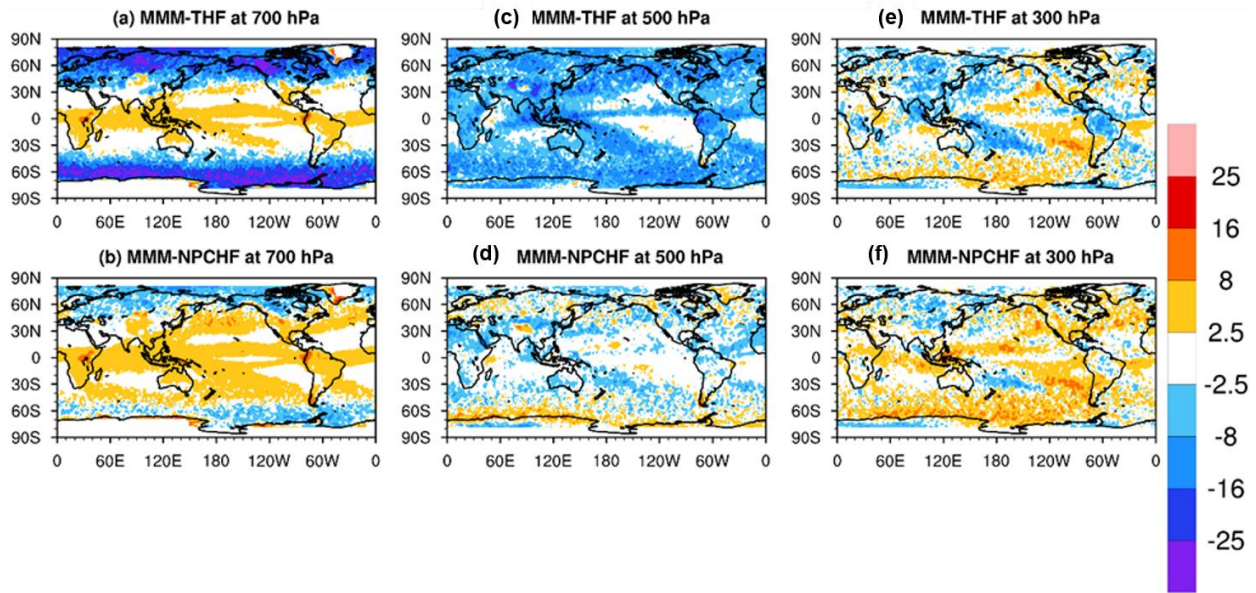


637

638 **Figure 6** continue.

639

640



641

642 **Figure 7.** (a) CMIP5 multi-model means (MMM) cloud fraction biases at 700 hPa against the  
643 estimated total hydrometeor fraction (THF), (b) same as (a) but against the estimated cloud-only  
644 hydrometeor fraction (NPCHF); (c)—(d) same as (a)—(b) but at 500 hPa; (e)—(f) same as (a)—  
645 (b) but at 300 hPa. Units: %.

646

647 **APPENDIX**

648 **TABLE**

649 **Table A1a.** Model label, number of model grids, institution and model full name of CMIP5  
 650 models examined in this study.

<b>Model Label</b>	<b>Number of model grids (x, y, and z)</b>	<b>Institution/Full Model Name</b>
GISS-E2-R	90x144x29	NASA / Goddard Institute for Space Studies, USA/GISS-E2-R
Inmcm4	120x180x21	Institute for Numerical Mathematics, Russia/Inmcm4
IPSL	96x96x39	Institute Pierre Simon Laplace, France/IPSL-CM5A-LR
MIROC	64x128x80	University of Tokyo, NIES, and JAMSTEC, Japan/MIROC-ESM-CHEM
MIROC-ESM	64x128x80	University of Tokyo, NIES, and JAMSTEC, Japan/MIROC-ESM
MRI-CGCM3	160x320x35	Meteorological Research Institute, Japan/MRI-CGCM3
NorESM	96x144x26	Norwegian Climate Centre, Norway/NorESM1-M
CSIRO	96x192x18	Australian Commonwealth Scientific and Industrial Research Organization, Australia/CSIRO-Mk3-6-0
MPI-ESM-LR	192x96x47	Max Planck Institute for Meteorology, Germany/MPI-ESM-LR

651

652 **Table A1b.** Outline of cloud microphysics and cloud fraction parameterizations used in the CMIP5  
653 models listed in Table A1a.

Models	Prognostic cloud variables	Bulk single moment or double moment	Cloud fraction (PDF based or Non-PDF based)	References
GISS-E2-R	Single mixing ratio of total water Diagnostic precipitating snow	Bulk single moment; mixing ratio of cloud condensate with temperature dependent partitioning (The bounds are adjustable constants with current settings of ice $T = -35^{\circ}\text{C}$ and liquid at $T = -4^{\circ}\text{C}$ over ocean; $T = -35^{\circ}\text{C}$ and liquid at $T = -10^{\circ}\text{C}$ over land).	Diagnostic, non-PDF based	<i>Del Genio et al. (1996)</i>
Inmcm4	Mixing ratio of cloud liquid and ice	Bulk single moment Large scale condensation in the case of relative humidity exceeds 1.	Diagnostic, non-PDF based	<i>Volodin et al., (2010)</i>
IPSL	Single mixing ratio of total water	Bulk single moment; mixing ratio of cloud condensate with temperature dependent partitioning (The bounds are adjustable constants with current settings ice at $T = -15^{\circ}\text{C}$ and liquid at $T = 0^{\circ}\text{C}$ ).	Diagnostic PDF based	<i>Bony and Emanuel (2001)</i>
MIROC and MIROC-ESM	Mixing ratio of cloud liquid and ice	Bulk single moment; different phases determined by temperature	Diagnostic PDF scheme with minor change for calculating anvil cloud	<i>Ogura et al. (2008)</i> <i>Le Treut and Li, (1991);</i> <i>Hourdin et al. (2006)</i>
MRI-CGCM3	Mixing ratio of cloud liquid and ice	Double moment scheme.	Diagnostic PDF based	<i>Tiedtke (1993)</i> <i>Yukimoto et al. (2011)</i>
NorESM1	Single mixing ratio of total water	Bulk single moment; mixing ratio of cloud condensate with temperature dependent	Diagnostic, non-PDF based	<i>Rashe and Kristjánsson (1998)</i>

		partitioning (The bounds are adjustable constants with current settings ice at T = -40oC and liquid at T = -10oC).		<i>Zhang et al. (2003)</i> <i>Boville et al. (2006)</i>
CSIRO-Mk3.6.0	Mixing ratio of cloud liquid and ice; Diagnostic precipitating snow	Bulk single moment; ice crystal number concentration is diagnosed; mixing ratio of cloud condensate with temperature dependent partitioning (The bounds are adjustable constants with current settings ice at T = -40°C );	Diagnostic, non-PDF based	<i>Rotstayn et al. (1997)</i> <i>Rotstayn et al. (2000)</i>
MPI-ESM-LR	Mixing ratio of cloud liquid and ice		cloud fraction is calculated diagnostically as a function of relative humidity	Sundqvist et al. ( <a href="#">1989</a> )

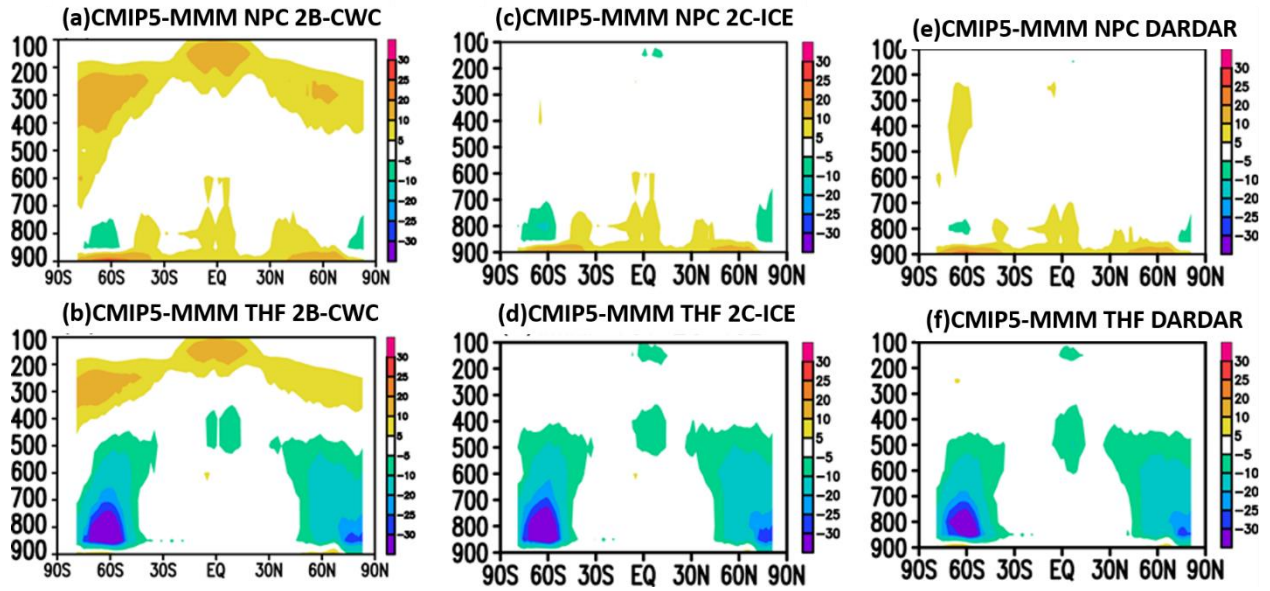
654

655

656

657

658



659

660 **Figure A1.** (a) CMIP5 multi-model-mean (MMM) zonally-averaged annual mean cloud fraction  
661 biases, compared to non-precipitating and non-convective (NPC) hydrometeor frequency (HF)  
662 estimated from 2B-CWC; (b) same as in (a) but against total radiatively-active hydrometeor  
663 frequency (ice+liquid+snow) (THF) from 2B-CWC; (c)—(d) same as in (a)—(b) but for 2C-ICE;  
664 (e)—(f) same as (a)—(b) but for DARDAR. Units: %.

665

666